

Nonequilibrium Probes of Quantum Geometry in Gapless Systems

Bastien Lapierre^{*1, 2}, Per Moosavi^{†3, 4}, and Blagoje Oblak^{‡5}

¹Department of Physics, Princeton University, Princeton, New Jersey, 08544, USA

²Philippe Meyer Institute, Physics Department, Ecole Normale Supérieure (ENS), Université PSL, 24 rue Lhomond, F-75231 Paris, France

³Department of Physics, Stockholm University, 10691 Stockholm, Sweden

⁴Institute for Theoretical Physics, ETH Zurich, Wolfgang-Pauli-Strasse 27, 8093 Zürich, Switzerland

⁵Université Claude Bernard Lyon 1, ICJ UMR5208, CNRS, 69622 Villeurbanne, France

November 12, 2025

Abstract

Much of our understanding of gapless many-body quantum systems stems from their low-energy descriptions as conformal field theories. This is especially true in 1+1 dimensions, where such theories have an infinite-dimensional parameter space induced by their conformal symmetry. We reveal the associated quantum geometry by considering finite systems driven by time-dependent conformal transformations. For small deformations, perturbation theory predicts absorption rates and linear responses that are intrinsically related to components of the quantum geometric tensor. For arbitrarily large but adiabatic deformations, we show that periodic drives give rise to nontrivial return amplitudes involving the quantum metric, beyond the familiar leading order that only features a Berry phase. Our field-theoretic findings are universal, comprising general relations between measurable quantities and quantum geometry that only depend on the central charge of the conformal symmetry. This is supported by both analytical results for quantum dynamics under certain Floquet drives, and numerical simulations of gapless lattice models.

^{*}bastien.lapierre@phys.ens.fr

[†]per.moosavi@fysik.su.se

[‡]oblak@math.univ-lyon1.fr

Contents

1	Introduction	3
1.1	Driven conformal field theory	3
1.2	Summary of results	5
1.3	Plan of the paper	7
2	Virasoro quantum geometry	7
2.1	Virasoro group theory	7
2.2	Unitary drives in CFT	9
2.3	Quantum geometric tensor in CFT	11
3	Perturbative quantum geometry	13
3.1	Virasoro quantum metric from absorption rates	14
3.2	Virasoro Berry curvature from linear response	15
4	Quantum geometry from adiabatic drives	16
4.1	Return amplitudes from group theory	17
4.2	Return probabilities for rotating drives	19
5	Rotating drives in $SL(2, \mathbb{R})$	21
5.1	Evolution operator	22
5.2	Nonlinear and linear responses	24
5.3	Return amplitudes and probabilities	25
6	Discussion	26
A	Brief dictionary of CFT formulas	27
B	Virasoro quantum geometry away from the identity	29
C	Linear response to Virasoro drives	30
D	Rotating $SL(2, \mathbb{R})$ drives	31
E	Lattice calculations	33
	References	35

1 Introduction

Half a century ago, a seminal paper [1, 2] by Arnold put forward the idea that fluid flows trace geodesics in an infinite-dimensional manifold, revealing the key role played by infinite-dimensional (metric) geometry in physics [3–5]. The geometry in such cases is classical, related to the phase space of the system and to the kinetic energy in the classical Hamiltonian. In recent years though, it has come to be appreciated that *quantum* geometry—the geometry of bundles of quantum states over various parameter spaces [6, 7]—is essential to a number of phenomena in atomic and condensed matter physics; see *e.g.* [8–16] or the recent review [17] and references therein. This notably includes instances of quantum fluids and other many-body systems whose low-energy description involves an infinite-dimensional parameter space, blending Arnold’s ideas with those of modern quantum geometry.

A natural question, then, is whether infinite-dimensional quantum geometry can have observable consequences. That the answer must be affirmative is supported by the fact that any many-body quantum system is described, at low energy, by a quantum field theory, whose phase space is necessarily infinite-dimensional. Coherent states on that phase space define a bundle with an infinite-dimensional quantum geometry, as desired. For instance, Bloch coherent states for a single spin are labeled by two coordinates on a sphere, but their cousins for spin chains are labeled by infinitely many parameters (two at each lattice site) in the thermodynamic limit. While infinite-dimensional quantum geometry is ubiquitous in that sense, the issue is to find a setup that is observable, suitably universal, and sufficiently tractable even beyond small perturbations in parameter space. This work aims to provide just such a universal description for gapless systems, supported by both analytical computations and numerics.

1.1 Driven conformal field theory

Our framework is that of conformal field theory (CFT) in one time and one space dimension (1+1D). In condensed matter, such models typically emerge as low-energy effective theories of gapless many-body quantum systems [18, 19]. What makes the setup both satisfyingly rich and tractable for our purposes is the emergence of a symmetry under conformal transformations, generated by an infinity of operators—the Fourier modes of the stress-energy tensor—that satisfy the commutation relations of the celebrated Virasoro algebra [20]. The key idea is to excite the system in a time-dependent manner that switches on operators that are normally silent in CFT, thereby probing directions in quantum parameter space that would not appear for homogeneous systems in equilibrium.

Concretely, consider a chiral CFT with stress-energy tensor $\mathcal{T}(x)$, evolving under the time-dependent Hamiltonian¹

$$H(t) = \int_0^L dx v_t(x) \mathcal{T}(x), \quad (1.1)$$

where the local velocity profile $v_t(x) > 0$ varies smoothly in space and time. Space and time coordinates are respectively $x \in [0, L]$ and $t \in \mathbb{R}$, with L the length (volume) of the system. We also impose periodicity in both space and time, namely $\mathcal{T}(x+L) = \mathcal{T}(x)$, $v_t(x+L) = v_t(x)$, and $v_{t+T}(x) = v_t(x)$, where T is the period of the drive. In standard CFT, the velocity profile would be homogeneous and constant: $v_t(x) = v = \text{const}$. By contrast, the Hamiltonian (1.1) is that of a chiral inhomogeneous CFT [21–26] with a time-dependent velocity profile $v_t(x)$ generalizing

¹Units are such that $\hbar = 1$ and velocity is dimensionless, *i.e.* expressed in units of the ‘speed of light’.

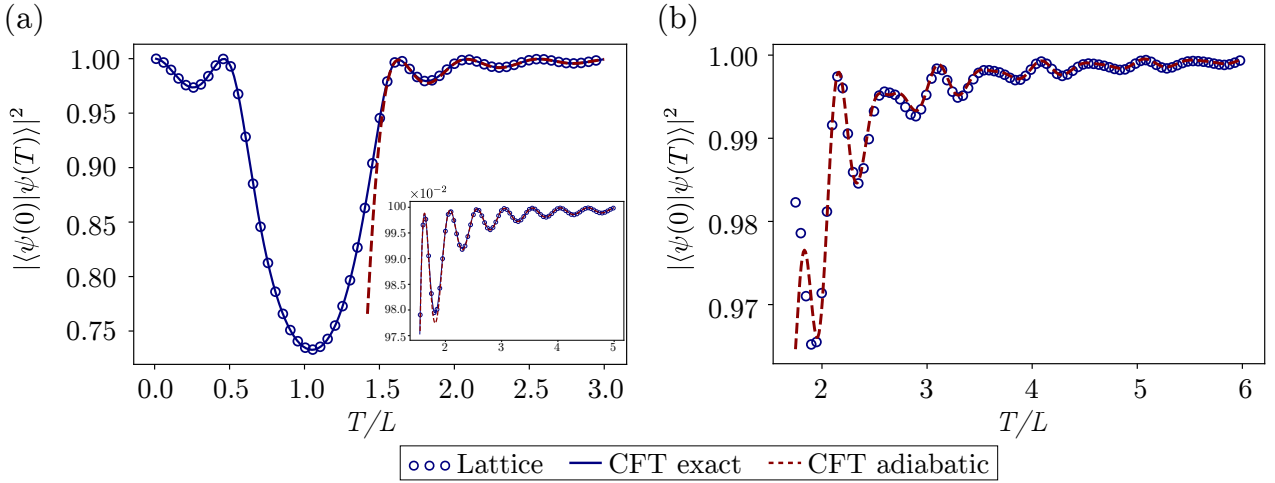


Figure 1: Return probability $|\langle \psi(0) | \psi(T) \rangle|^2$, starting from the initial ground state $|\psi(0)\rangle$ under the driven Hamiltonian (1.1) (extended to both right and left movers), plotted as a function of the (dimensionless) period T/L for two different velocity profiles. (a) Velocity $v_t(x) = \cosh(2\lambda) - \sinh(2\lambda) \cos(2\pi k[x/L - t/T])$ for $\lambda = 0.15$ and a single harmonic $k = 2$. This profile only involves a finite-dimensional subalgebra of the Virasoro algebra, so the return probability can be evaluated exactly for any driving period (blue curve). (b) Velocity $v_t(x) = v[\cosh(2\lambda) - \sinh(2\lambda) \cos(2\pi k[x/L - t/T]) + \frac{1}{5} \sin(2\pi k'[x/L - t/T])]$ for $\lambda = 0.15$, two harmonics $k = 2, k' = 3$, and a normalization factor v . This profile involves the full infinite-dimensional Virasoro algebra, so no exact general expression is available for the return probability. In both cases, the return probability goes to 1 in the adiabatic limit $T/L \rightarrow \infty$. For finite T/L , this behavior is corrected by small oscillations whose amplitude is essentially the squared quantum distance between two nearby coherent states (dashed purple curves). When T/L decreases, oscillations become more pronounced and are eventually no longer related to the quantum metric. The blue dots are the corresponding numerical simulations of the spin chain (1.2) illustrated in Fig. 2 with $\Delta = 0$ and couplings $J_j(t) \propto v_t(x_j)$ for $N = 400$ sites x_j (see Appendix E). Note the remarkable agreement between numerics and our analytical CFT results.

earlier Floquet setups [27–33]. This extra, more general time-dependence will ultimately allow us to probe the quantum geometry of the system, as exemplified in Fig. 1.

Concentrating on chiral CFTs with spatial periodicity is motivated not only by the simpler presentation, but also by its general applicability. Indeed, the setting is straightforwardly extended to the nonchiral case of decoupled right and left movers arising in many applications with periodic boundary conditions. An important example is provided by spin chains, whose low-energy excitations are described by the nonchiral version of (1.1). Think *e.g.* of an XXZ spin chain with N sites and Hamiltonian

$$H_{\text{XXZ}}(t) = - \sum_{j=1}^N J_j(t) \left[S_j^x S_{j+1}^x + S_j^y S_{j+1}^y - \Delta S_j^z S_{j+1}^z \right] \quad (|\Delta| < 1), \quad (1.2)$$

with $\mathfrak{su}(2)$ generators $S_j^{x,y,z} \equiv S_{j+N}^{x,y,z}$ in the spin-1/2 representation at site j , and time-dependent couplings $J_j(t) > 0$ that vary on mesoscopic length scales² and satisfy $J_j(t) = J_j(t + T)$ and $J_j(t) = J_{j+N}(t)$. See Fig. 2 for an illustration. In addition, our setting can describe systems with open boundaries by folding/unfolding techniques adapted to inhomogeneous CFT [34–36].

²‘Mesoscopic’: on scales much larger than the lattice spacing L/N but much smaller than the system size L .

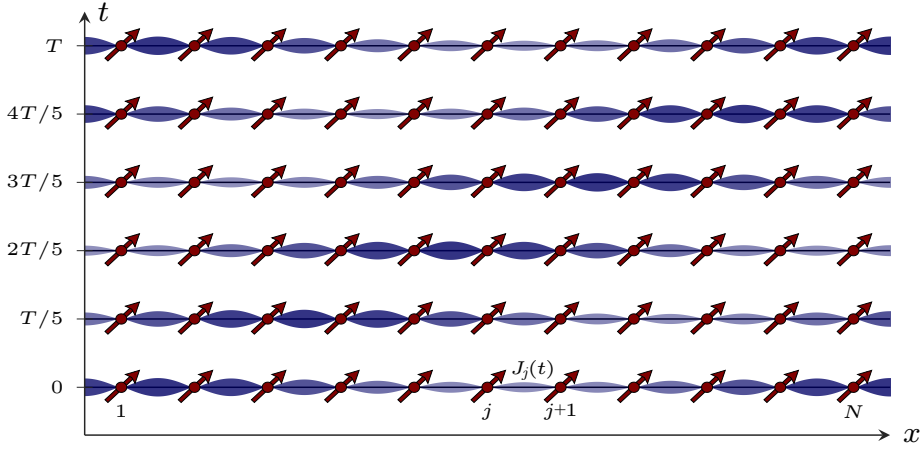


Figure 2: Cartoon of a periodically driven gapless spin chain (1.2) of length $L \propto N$, with periodic boundary conditions. The inhomogeneous couplings $J_j(t)$ vary in space on mesoscopic length scales, and they vary smoothly in time with period T .

Related questions on quantum geometry in CFT have recently been studied in holography [37–41] and quantum complexity [42–44]. Note, however, that many of the tools in this paper apply to a wide variety of quantum systems, well beyond CFT. Indeed, part of our work boils down to unitary representations of continuous groups, and the way these can be used to build time-dependent Hamiltonians. One instance is the family of Hamiltonians (1.1) for the Virasoro symmetry group of CFT, but many other physical systems fall into the same framework. Examples include the group $SU(2)$ describing a spin in a rotating magnetic field [45], or the special linear group $SL(2, \mathbb{R})$ describing both squeezed states in quantum optics [46] and Hall viscosity [47, 48]. In fact, a close cousin of the chiral theory (1.1) investigated here is the Hamiltonian of edge modes of quantum Hall droplets subjected to time-dependent area-preserving deformations [49–51].

1.2 Summary of results

In studying CFT Hamiltonians of the form (1.1), we obtain general results split into two categories: *perturbative* and *adiabatic*; see Fig. 3. These are universal in that they provide low-energy relations between measurable quantities and quantum geometry, which only depend on the central charge of the emergent effective description.

- On the perturbative end (Sec. 3), we consider velocities that only deviate slightly from a constant $v_0 > 0$, namely

$$v_t(x) = \begin{cases} v_0 & \text{for } t < 0, \\ v_0 + \epsilon w_t(x) & \text{for } t \geq 0, \end{cases} \quad (1.3)$$

where $\epsilon \ll 1$ and $w_t(x)$ is smooth but otherwise arbitrary. The resulting Hamiltonian (1.1) is close to that of a homogeneous CFT, so familiar formulas on time-dependent perturbation theory apply (provided L is kept finite). In particular, picking $w_t(x) = \omega^{-1} \cos(\omega t) \partial_x X(x)$ with frequency $\omega > 0$ and a time-independent function $X(x)$ yields an absorption rate $\Gamma(\omega)$ induced by transitions from the CFT ground state to excited states. We compute this rate and show, following [52], that its integral over frequencies

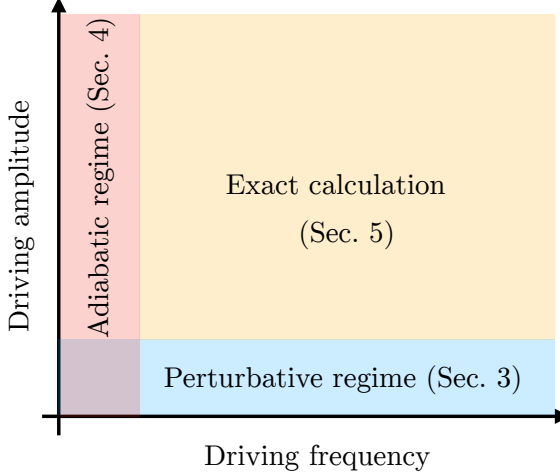


Figure 3: The different regimes of interest in this work: drives in the perturbative regime are those for which the function $v_t(x)$ in Eq. (1.1) is close to being uniform, and drives in the adiabatic regime are those for which $v_t(x)$ oscillates slowly with t . When available, exact solutions cover the entire parameter space, but they are limited to specific families of deformations.

is proportional to the quantum metric. In formulas,

$$\int_0^\infty d\omega \Gamma(\omega) \sim \frac{\epsilon^2}{2L^2} \mathcal{G}(\mathbf{X}, \mathbf{X}) \quad (1.4)$$

to leading order in ϵ , where $\mathcal{G}(\cdot, \cdot)$ is the quantum metric evaluated at the identity in an infinite-dimensional space of inhomogeneous coherent states.

Another natural quantity to investigate is the response of stress-energy expectation values to the perturbation (1.3). In that context, we pick an arbitrary (smooth) L -periodic function $Y(x)$, and ask how the time-dependent expectation value of $\mathcal{O} = \int dx Y(x) \mathcal{T}(x)$ differs from its equilibrium value. We show that

$$\langle \mathcal{O} \rangle(t) - \langle \mathcal{O} \rangle \sim \epsilon \int_0^t ds \partial_t \mathcal{F}(\mathbf{Y}_{t-s}, \mathbf{X}_s) \quad (1.5)$$

to leading order in ϵ , where $\mathbf{Y}_t \equiv Y(x + t) \partial_x$ and $\mathcal{F}(\cdot, \cdot)$ is the Berry curvature evaluated at the identity in the same infinite-dimensional parameter space as the metric in Eq. (1.4).

- On the adiabatic end (Sec. 4), we consider Hamiltonians (1.1) whose velocity profile $v_t(x)$ is well away from a constant, but varies slowly in time t compared to the system size. We assume that the system is initially prepared in its ground state $|\psi(0)\rangle$, and investigate its overlap with the state $|\psi(T)\rangle$ at the end of an adiabatic cycle. To leading order in the adiabatic limit, the only difference between $|\psi(0)\rangle$ and $|\psi(T)\rangle$ is an overall phase—the sum of a dynamical phase and a Berry phase [53]. But, beyond leading order, there are new subleading corrections in the adiabatic parameter $\delta \sim L/T \ll 1$. Our interest lies in these corrections: we show that they probe the quantum metric of the space of conformal frames—the same metric as in the integrated absorption rate (1.4). In formulas, the return probability (Loschmidt echo) is

$$|\langle \psi(0) | \psi(T) \rangle|^2 \sim 1 - \delta^2 \mathcal{G}(\mathbf{Y}, \mathbf{Y}), \quad (1.6)$$

where $\delta\mathbf{Y}$ is a small vector field measuring the deviation between the rays of $|\psi(T)\rangle$ and $|\psi(0)\rangle$.³ We compute this deviation exactly for ‘rotating drives’ of the form $v_t(x) = v(x - \omega t)$, with a driving frequency $\omega = 2\pi/T$ and a given profile $v(x)$ at $t = 0$. The resulting return probability (1.6) gives rise to the oscillating pattern in Fig. 1.

We stress that all these results are expansions, in different limiting regimes, of the same unified picture; see Fig. 3. However, access to the full range of drives is generally only possible via exact analytical computations for special classes of conformal transformations. These are studied in Sec. 5, and used there to benchmark our limiting results. An example is displayed in Fig. 1(a), showing excellent agreement between exact CFT return probabilities, their adiabatic expansions, and the corresponding numerical lattice computations.

1.3 Plan of the paper

The organization of the paper reflects the thematic split outlined above. In Sec. 2, we introduce the family of CFT Hamiltonians (1.1) and their quantum geometry. Sec. 3 relates this to observable results (such as transition rates and linear-response coefficients) for small perturbations (1.3). Sec. 4 concerns large but adiabatically driven deformations, and the general behavior of the return probability exemplified in Fig. 1 is derived for the important class of rotating drives. In Sec. 5, we present families of time-dependent deformations that can be solved exactly using finite-dimensional matrices, without resorting to expansions in different limiting regimes. We conclude in Sec. 6, listing some natural extensions and follow-ups. Some technical details are deferred to appendices.

2 Virasoro quantum geometry

This section introduces the quantum geometry of the emergent conformal symmetry of gapless quantum systems, phrased within the context of CFT. We first recall some basics of conformal transformations and Virasoro group theory, then introduce inhomogeneous CFT and coherent states, and finally turn to our main act: the quantum geometry of CFT.

2.1 Virasoro group theory

We begin by reviewing conformal transformations in any 1+1D CFT. The presentation starts from the *group* of conformal transformations and introduces their *algebra* as a second step.⁴ Select formulas are summarized in Appendix A.

Conformal maps. Our setup is a 1+1D CFT describing the low-energy dynamics of a gapless many-body quantum system. For definiteness, consider the theory on a Lorentzian cylinder with time coordinate $t \in \mathbb{R}$ and spatial coordinate $0 \leq x \leq L$, which we will mostly trade for the angle $\varphi \equiv 2\pi x/L$. The spacetime metric reads $ds^2 = -dt^2 + dx^2 = -dt^2 + (L/2\pi)^2 d\varphi^2$, with the ‘speed of light’ set to one. The corresponding conformal group is (up to a zero-mode) a direct product $\text{Diff}(S^1) \times \text{Diff}(S^1)$ [56], where $\text{Diff}(S^1)$ is (the universal cover of) the group of

³This vector field \mathbf{Y} has nothing to do with the one in the linear response formula (1.5).

⁴Due to its infinite dimension, representations of the Virasoro group should strictly speaking be built the other way around: starting from the algebra and integrating to the group [54, 55]. We deliberately deviate from this, since our presentation allows one to directly generalize the approach to any quantum system with a (finite-dimensional) continuous symmetry group, where properties such as existence are less of an issue.

orientation-preserving diffeomorphisms of the circle S^1 . Specifically, conformal transformations can be expressed in light-cone coordinates $\varphi^\pm = \varphi \pm 2\pi t/L$ as

$$\varphi^- \mapsto f(\varphi^-), \quad \varphi^+ \mapsto \bar{f}(\varphi^+), \quad (2.1)$$

where f is any smooth real function that satisfies

$$f'(\varphi) > 0 \quad \text{and} \quad f(\varphi + 2\pi) = f(\varphi) + 2\pi, \quad (2.2)$$

and similarly for \bar{f} . The group operation in $\text{Diff}(S^1)$ is given by composition $(f \circ g)(\varphi) = f(g(\varphi))$, the identity element is $\mathbb{I}(\varphi) = \varphi$, and f^{-1} denotes the inverse of f .

Since right- and left-moving conformal transformations commute, one may restrict attention to a single chirality, *i.e.* deal with f alone (rather than a pair f, \bar{f}). Time translations and rotations then take the same form $f(\varphi) = \varphi + \text{const}$, as follows *e.g.* from the definition of the right-moving light-cone coordinate φ^- in Eq. (2.1). This applies both to chiral systems and to nonchiral systems with periodic boundary conditions. (For nonchiral systems with *e.g.* Neumann boundary conditions, right and left movers are coupled at the boundaries, but the theory can be unfolded to a chiral one on a cylinder with twice the circumference.)

Let \mathcal{H} denote the Hilbert space of the CFT. In quantum theory, symmetry transformations are typically implemented by unitary operators. This also holds for conformal transformations $f \in \text{Diff}(S^1)$, which act on \mathcal{H} through unitary operators $U(f)$ [54, 55]. These furnish a unitary representation of $\text{Diff}(S^1)$, albeit a projective one. Indeed,

$$\mathcal{U}(f)\mathcal{U}(g) = e^{ic\mathcal{C}(f,g)}\mathcal{U}(f \circ g), \quad (2.3)$$

where the parameter $c > 0$ is the central charge of the CFT, and the functional

$$\mathcal{C}(f, g) \equiv \oint \frac{d\varphi}{48\pi} \log[f'(g(\varphi))] \frac{g''(\varphi)}{g'(\varphi)} \quad (2.4)$$

is known as the Bott cocycle; see *e.g.* [4]. Here and elsewhere, a prime $'$ denotes differentiation with respect to φ and $\oint d\varphi$ means $\int_0^{2\pi} d\varphi$. Note that $\mathcal{U}(f^{-1}) = \mathcal{U}(f)^{-1}$ since $\mathcal{C}(f, f^{-1}) = 0$.

Virasoro algebra. An infinitesimal conformal map is a function $f(\varphi) = \varphi + \epsilon X(\varphi)$, where $\epsilon \ll 1$ and $\mathbf{X} = X(\varphi)\partial_\varphi$ is a real vector field with $X(\varphi + 2\pi) = X(\varphi)$. Thus, the Lie algebra of $\text{Diff}(S^1)$ is the space $\text{Vect}(S^1)$ of vector fields on the circle endowed with the standard Lie bracket $[X\partial_\varphi, Y\partial_\varphi] \equiv (XY' - YX')\partial_\varphi$.⁵ We expand them in Fourier modes $\hat{X}_m = \hat{X}_{-m}^*$ as

$$\mathbf{X} = \sum_{m \in \mathbb{Z}} \hat{X}_m e^{im\varphi} \partial_\varphi. \quad (2.5)$$

In quantum theory, infinitesimal conformal transformations are represented by anti-Hermitian operators

$$\mathbf{u}(\mathbf{X}) \equiv \partial_\epsilon \mathcal{U}(\mathbb{I} + \epsilon \mathbf{X}) \Big|_{\epsilon=0} \equiv -i \oint d\varphi X(\varphi) \mathcal{T}(\varphi), \quad (2.6)$$

⁵To find this bracket, take infinitesimal deformations $f(\varphi) = \varphi + \epsilon X(\varphi)$ and $g(\varphi) = \varphi + \epsilon Y(\varphi)$, and expand their commutator $f \circ g - g \circ f^{-1} \circ g^{-1}$ in ϵ and ϵ .

which defines the (Hermitian) stress-energy tensor $\mathcal{T}(\varphi)$. The latter is indeed the generator of conformal transformations, and may be seen as an operator-valued distribution $\mathcal{T}(\theta) = i\mathfrak{u}(\delta(\varphi - \theta)\partial_\varphi)$, with $\delta(\varphi)$ the 2π -periodic delta function. Expanded in Fourier modes,

$$\mathcal{T}(\varphi) = \frac{1}{2\pi} \sum_{n \in \mathbb{Z}} e^{in\varphi} \left(L_n - \frac{c}{24} \delta_{n,0} \right) \quad \text{with} \quad L_m \equiv i\mathfrak{u}(e^{-im\varphi}\partial_\varphi) + \frac{c}{24} \delta_{m,0}, \quad (2.7)$$

using which Eq. (2.6) becomes

$$\mathfrak{u}(\mathbf{X}) = -i \sum_m \hat{X}_m \left(L_{-m} - \frac{c}{24} \delta_{m,0} \right). \quad (2.8)$$

The operators L_m obtained in this way satisfy $L_m^\dagger = L_{-m}$ and the commutation relations

$$[L_m, L_n] = (m - n)L_{m+n} + \frac{c}{12}m(m^2 - 1)\delta_{m+n,0} \quad (2.9)$$

of the Virasoro algebra, consistent with the projective composition law (2.3) (see Appendix A).

2.2 Unitary drives in CFT

We now turn to the action of conformal transformations and show how this allows one to construct parameter-dependent CFT Hamiltonians, each labeled by a choice of ‘conformal frame’.

Inhomogeneous CFT. In any (chiral) 1+1D CFT, time translations are generated by the zero mode of the stress-energy tensor (2.7), so the standard CFT Hamiltonian is

$$H_0 = \frac{2\pi}{L} \oint d\varphi \mathcal{T}(\varphi) = \frac{2\pi}{L} \left(L_0 - \frac{c}{24} \right). \quad (2.10)$$

We refer to it as the *undeformed* or *homogeneous* Hamiltonian, in the sense that it is the Hamiltonian of the theory viewed from a suitable ‘rest frame’. Indeed, in CFT, observers are free to perform conformal changes of coordinates (2.1) and measure energy from a different ‘conformal frame’. (This is similar to special relativity, where Lorentz boosts affect the value of energy.) We therefore refer to the Hamiltonian in a different frame labeled by $f \in \text{Diff}(S^1)$, namely

$$H[f] \equiv \mathcal{U}(f) H_0 \mathcal{U}(f)^{-1}, \quad (2.11)$$

as the CFT Hamiltonian *deformed* by f . This construction forms our starting point: viewing each operator (2.11) as being labeled by a *conformal frame* $f \in \text{Diff}(S^1)$, we will investigate the quantum geometry of the resulting bundle of eigenstates. The underlying parameter space is a quotient

$$\mathcal{M} \cong \text{Diff}(S^1)/S^1, \quad (2.12)$$

since the undeformed Hamiltonian (2.10) commutes with L_0 but fails to commute with any other Virasoro generator, as is clear from the algebra (2.9).⁶

⁶The notation $\text{Diff}(S^1)/S^1$ is standard for the space of all S^1 diffeomorphisms modulo rotations (see *e.g.* [57]). Technically, we should instead write $\text{Diff}(S^1)/\mathbb{R}$, since our notation ‘ $\text{Diff}(S^1)$ ’ refers to the universal cover of the diffeomorphism group of the circle. We stick to the standard notation nevertheless.

As mentioned in Sec. 1, our strategy is to probe the geometry of parameter space by considering conformal transformations $f_t(\varphi)$ that vary in time t . The result is a CFT governed by a time-dependent deformed Hamiltonian

$$H[f_t] = \mathcal{U}(f_t) H_0 \mathcal{U}(f_t)^{-1} = \frac{2\pi}{L} \oint d\varphi \mathcal{U}(f_t) \mathcal{T}(\varphi) \mathcal{U}(f_t)^{-1}, \quad (2.13)$$

where we used Eq. (2.10). This operator can be made explicit by relying on the usual transformation law of the CFT stress-energy tensor,

$$\mathcal{U}(f) \mathcal{T}(\varphi) \mathcal{U}(f)^{-1} = [f'(\varphi)]^2 \mathcal{T}(f(\varphi)) - \frac{c}{24\pi} \{f, \varphi\} \quad (2.14)$$

involving the Schwarzian derivative $\{f, \varphi\} \equiv \frac{f'''}{f'} - \frac{3}{2} \left(\frac{f''}{f'} \right)^2$. Plugging this into Eq. (2.13) yields

$$H[f_t] = \frac{2\pi}{L} \oint \frac{d\varphi}{(f_t^{-1})'(\varphi)} \mathcal{T}(\varphi) + C[f_t], \quad (2.15)$$

where $C[f] \equiv -\frac{c}{12L} \oint d\varphi \{f, \varphi\}$ is a real number. The key point is that Eq. (2.15) takes the form of a time-dependent inhomogeneous CFT (1.1), with the (dimensionless) velocity profile $v_t(x) \equiv V_t(\varphi) = 1/(f_t^{-1})'(\varphi)$ and the identification $\mathcal{T}(x) \equiv (2\pi/L)^2 \mathcal{T}(\varphi)$ for $\varphi = 2\pi x/L$. Clearly, such deformations of the homogeneous theory (2.10) leave a huge amount of legroom: by suitably choosing the maps $f_t(\varphi)$, one can obtain essentially any profile $v_t(x)$. The only requirements are $v_t(x) > 0$ and the normalization $\frac{1}{L} \int_0^L \frac{dx}{v_t(x)} = \frac{1}{2\pi} \oint \frac{d\varphi}{V_t(\varphi)} = 1$, due to the conditions (2.2).

Virasoro coherent states. The parameter dependence of the Hamiltonian (2.11) entails a similar dependence for its eigenstates. For definiteness, we focus on coherent states, which are essentially obtained by acting with conformal transformations on a primary state. The latter is, by definition, a normalized state $|h\rangle$ in \mathcal{H} labeled by a conformal weight $h > 0$ and satisfying

$$L_0|h\rangle = h|h\rangle \quad \text{and} \quad L_m|h\rangle = 0 \quad \text{for all } m > 0. \quad (2.16)$$

Such a state can be obtained from the CFT vacuum $|0\rangle$, defined by $L_m|0\rangle = 0$ for all $m \geq -1$, by acting on it with the corresponding primary field; see *e.g.* [58]. For our purposes, we may assume that there is at least one primary state in the theory, as our results can equally well be stated for the vacuum by setting $h = 0$.

Given a primary state $|h\rangle$, it is standard practice to build a highest-weight representation of the Virasoro algebra (2.9), analogously to highest-weight representations of simple Lie algebras.⁷ We assume that the representation is unitary, so that $h \geq 0$. Within that representation, the spectrum of L_0 is $\{h, h+1, h+2, h+3, \dots\}$, so $|h\rangle$ is effectively a nondegenerate ground state with a (finite-volume) gap separating it from higher-energy states. Our bundle of *Virasoro coherent states* can then be constructed by acting on $|h\rangle$ with finite conformal transformations:

$$\mathcal{U}(f)|h\rangle \quad \text{for } f \in \text{Diff}(S^1). \quad (2.17)$$

Each of these is a normalized, nondegenerate eigenstate of the deformed Hamiltonian (2.11) with energy $(2\pi/L)(h - c/24)$ and a (finite-volume) gap above it. Such states are coherent in the same sense as Bloch coherent states or squeezed states in quantum optics [46], where the group $\text{Diff}(S^1)$ would respectively be replaced by $\text{SU}(2)$ or $\text{SL}(2, \mathbb{R})$.

⁷Technically, the representation is *lowest*-weight, but the highest-weight terminology is standard.

2.3 Quantum geometric tensor in CFT

Having introduced the family of coherent states (2.17), let us write their quantum geometric tensor. The latter consists of a metric and a Berry curvature. We first recall the definition of these concepts in a broader setting, then specialize to the Virasoro case.

Generalities on quantum geometry. Consider the Hilbert space \mathcal{H} of some quantum system. Given any nonzero state vector $|\psi\rangle \in \mathcal{H}$, let $[\psi] \equiv \{\lambda|\psi\rangle : \lambda \in \mathbb{C}\}$ be its ray in \mathcal{H} . Denote by $\mathbb{P}\mathcal{H} = (\mathcal{H} \setminus \{0\})/\mathbb{C}$ the corresponding complex projective space, *i.e.* the space of rays. Let the Hamiltonian $H[p]$ depend on some set of continuous parameters that label a point p in some parameter manifold \mathcal{M} . Finally, let $|\phi(p)\rangle \in \mathcal{H}$ be a normalized eigenstate of $H[p]$, with a dependence on p that we assume to be continuous. Then there is a well-defined (smooth) map

$$\mathcal{M} \rightarrow \mathbb{P}\mathcal{H} : p \mapsto [\phi(p)], \quad (2.18)$$

sending a set p of parameters on the corresponding ray. This map essentially defines the quantum geometry of \mathcal{M} . Indeed, $\mathbb{P}\mathcal{H}$ is a Kähler manifold equipped with a metric and a compatible symplectic form, so their pullback by the map in Eq. (2.18) yields a (possibly degenerate) *quantum metric* \mathcal{G} and a (possibly degenerate) *Berry curvature* \mathcal{F} on \mathcal{M} . These pullbacks are respectively given by the (symmetric) real and (antisymmetric) imaginary parts of the quantum geometric tensor $\mathcal{Q} \equiv \langle d\phi| \otimes |d\phi\rangle - \langle d\phi| \phi \rangle \otimes \langle \phi| d\phi\rangle$, where d is the exterior derivative on \mathcal{M} [6].⁸ Thus, the metric and Berry curvature read

$$\mathcal{G} = \langle d\phi| \odot |d\phi\rangle - \langle d\phi| \phi \rangle \odot \langle \phi| d\phi\rangle, \quad \mathcal{F} = -2i\langle d\phi| \wedge |d\phi\rangle, \quad (2.19)$$

where $T_1 \odot T_2 \equiv (T_1 \otimes T_2 + T_2 \otimes T_1)/2$ and $T_1 \wedge T_2 \equiv (T_1 \otimes T_2 - T_2 \otimes T_1)/2$ respectively denote the symmetrized and antisymmetrized tensor products.

A special case of interest for us occurs when parameter dependence stems from a unitary group action, as in the deformed Hamiltonian (2.11). Specifically, let G be a Lie group (with Lie algebra \mathfrak{g}); let \mathcal{U} be a (possibly projective) unitary representation of G in \mathcal{H} , and let the parameter-dependent Hamiltonian read $H[f] = \mathcal{U}(f)H_0\mathcal{U}(f)^{-1}$, where H_0 is again some ‘undeformed’ reference Hamiltonian. This would exactly happen for rotating spins or squeezed states, in which case $G = \text{SU}(2)$ or $G = \text{SL}(2, \mathbb{R})$, respectively. The underlying parameter space is a quotient similar to (2.12),

$$\mathcal{M} \cong G/G_0, \quad (2.20)$$

where G_0 is the subgroup of G whose elements leave H_0 unchanged. For both Bloch coherent states and squeezed states, this stabilizer G_0 is the group $\text{SO}(2) \cong S^1$, respectively yielding a parameter space that is a sphere $S^2 \cong \text{SU}(2)/S^1$ or a (hyperbolic) plane $\mathbb{R}^2 \cong \text{SL}(2, \mathbb{R})/S^1$.

Now choose some (isolated, nondegenerate) eigenstate $|h\rangle$ of H_0 , and replace the parameter-dependent eigenstates $|\phi(p)\rangle$ in (2.18) by the states $\mathcal{U}(f)|h\rangle$, as in Eq. (2.17). The resulting metric and Berry curvature (2.19) are readily found thanks to the unitarity relation $\mathcal{U}(f)^{-1} = \mathcal{U}(f)^\dagger$, and they can be expressed in terms of the Lie algebra representation defined similarly to Eq. (2.6), namely $\mathfrak{u}(\mathbf{X}) \equiv \partial_\epsilon \mathcal{U}(\mathbb{I} + \epsilon \mathbf{X})|_{\epsilon=0}$ for $\mathbf{X} \in \mathfrak{g}$. When evaluated at the identity

⁸One should understand the definition of \mathcal{Q} as follows: given a point $p \in \mathcal{M}$ and paths $\gamma(t), \chi(s) \in \mathcal{M}$ such that $\gamma(0) = \chi(0) = p$, the quantum geometric tensor takes the two tangent vectors $\partial_t \gamma|_{t=0}, \partial_s \chi|_{s=0}$ to return the complex number $\mathcal{Q}(\partial_t \gamma|_{t=0}, \partial_s \chi|_{s=0}) \equiv \partial_s \partial_t [\langle \phi(\chi(s))| \phi(\gamma(t)) \rangle - \langle \phi(\chi(s))| \phi(p) \rangle \langle \phi(p)| \phi(\gamma(t)) \rangle]|_{t=s=0}$. This definition is independent of the choice of normalized representatives $|\phi(p)\rangle$ for the rays in Eq. (2.18).

coset labeled by $f = \mathbb{I}$ in parameter space (2.20), the metric and the curvature with arguments $\mathbf{X}, \mathbf{Y} \in \mathfrak{g}$ read

$$\mathcal{G}(\mathbf{X}, \mathbf{Y}) = -\frac{1}{2}\langle h | \{ \mathbf{u}(\mathbf{X}), \mathbf{u}(\mathbf{Y}) \} | h \rangle + \langle h | \mathbf{u}(\mathbf{X}) | h \rangle \langle h | \mathbf{u}(\mathbf{Y}) | h \rangle, \quad (2.21a)$$

$$\mathcal{F}(\mathbf{X}, \mathbf{Y}) = i\langle h | [\mathbf{u}(\mathbf{X}), \mathbf{u}(\mathbf{Y})] | h \rangle, \quad (2.21b)$$

where $\{ \cdot, \cdot \}$ and $[\cdot, \cdot]$ respectively denote the anticommutator and the commutator of operators in \mathcal{H} . Note that we are abusing notation: the arguments of the quantum geometric tensor are tangent vectors of the manifold (2.20), not Lie algebra elements. The reason this is harmless is because both lines in Eq. (2.21) vanish when either \mathbf{X} or \mathbf{Y} belong to the Lie algebra of the stabilizer G_0 , and because \mathbf{X}, \mathbf{Y} do in fact define unique tangent vectors of the quotient space G/G_0 . Even so, both the metric and the curvature are generally degenerate on the manifold (2.20), though they can be nondegenerate on further quotient spaces thereof. We will see examples of this below (no such complications arise for Bloch coherent states or squeezed states).

The quantum metric and the Berry curvature can similarly be evaluated at any other point fG_0 in parameter space (2.20). In fact, they are fully determined by their expression (2.21) at the identity coset. The only difference is that the Lie algebra elements \mathbf{X}, \mathbf{Y} of Eq. (2.21) are then replaced by images of the Maurer-Cartan form acting on tangent vectors at f . This is to say that the quantum geometric tensor is invariant under G , which here stems from the form $\mathcal{U}(f)H_0\mathcal{U}(f)^{-1}$ of the deformed Hamiltonian, with unitary \mathcal{U} . See Appendix B for details, which we omit here since these expressions will seldom be needed below.

Virasoro quantum geometry. The formulas in Eq. (2.21) readily apply to the Virasoro coherent states of Sec. 2.2. In practice, the only complication is that the group $G = \text{Diff}(S^1)$ is now infinite-dimensional, so any tensor field on G is a functional of a function $f(\varphi)$. What simplifies matters is that these tensor fields are invariant under $\text{Diff}(S^1)$, hence wholly determined by their expression at the identity $\mathbb{I}(\varphi) = \varphi$. For this reason, we now describe the quantum geometric tensor of CFTs by focusing entirely on Eq. (2.21) at the identity. Minimal effort is then needed to extend the result to fully fledged tensor fields on the entire group manifold, but this last bit is less essential for us and is relegated to Appendix B for brevity.

Consider first the ingredients needed in Eq. (2.21): \mathbf{X}, \mathbf{Y} are vector fields on the circle, the Lie algebra representation \mathbf{u} is the one in Eq. (2.6), and $|h\rangle$ is the highest-weight state introduced in Eq. (2.16). Fourier expanding $\mathbf{u}(\mathbf{X}), \mathbf{u}(\mathbf{Y})$ as in Eq. (2.7) and using the highest-weight conditions (2.16) then yields

$$\mathcal{G}(\mathbf{X}, \mathbf{Y}) = \sum_{m \in \mathbb{Z}} |m| \left(h + \frac{c}{24}(m^2 - 1) \right) \hat{X}_{-m} \hat{Y}_m \equiv \sum_{m, n \in \mathbb{Z}} \mathcal{G}_{m,n} \hat{X}_m \hat{Y}_n, \quad (2.22a)$$

$$\mathcal{F}(\mathbf{X}, \mathbf{Y}) = -2i \sum_{m \in \mathbb{Z}} m \left(h + \frac{c}{24}(m^2 - 1) \right) \hat{X}_{-m} \hat{Y}_m \equiv \sum_{m, n \in \mathbb{Z}} \mathcal{F}_{m,n} \hat{X}_m \hat{Y}_n, \quad (2.22b)$$

where the respective components of the metric and the Berry curvature are

$$\mathcal{G}_{m,n} = \frac{1}{2} \langle h | \{ L_{-m}, L_{-n} \} | h \rangle - \langle h | L_{-m} | h \rangle \langle h | L_{-n} | h \rangle = |m| \left(h + \frac{c}{24}(m^2 - 1) \right) \delta_{m+n,0}, \quad (2.23a)$$

$$\mathcal{F}_{m,n} \equiv -i \langle h | [L_{-m}, L_{-n}] | h \rangle = 2im \left(h + \frac{c}{24}(m^2 - 1) \right) \delta_{m+n,0}. \quad (2.23b)$$

That there are infinitely many such components reflects the fact that parameter space is infinite-dimensional. That all these components vanish when $m = 0$ or $n = 0$ reflects the fact that parameter space is a quotient (2.12). Both the metric and the curvature are nondegenerate on the manifold (2.12) if $h > 0$; by contrast, if $h = 0$, the directions $m = \pm 1$ become degenerate due to the vanishing factor $m^2 - 1$. This reflects the fact that the quantum geometry of coherent states (2.17) is that of a coadjoint orbit [59]—in the case at hand, an orbit of the Virasoro group. Finally, that the components (2.23) are identical up to an absolute value of $m \in \mathbb{Z}$ in the metric (and a trivial rescaling) reflects the fact that the quantum geometry on the manifold (2.12) is Kähler, as is indeed the case for Virasoro coadjoint orbits [4, 57]. This Kähler property is also true for Bloch coherent states and squeezed states, of which our current setup is an infinite-dimensional analogue.

While it is convenient to write the metric and Berry curvature in terms of Fourier modes as in Eq. (2.22), it is also possible to express them as functionals of local vector fields. For the curvature, this can be done *e.g.* by inverse Fourier transforming Eq. (2.22b), which yields

$$\mathcal{F}(\mathbf{X}, \mathbf{Y}) = -2 \oint \frac{d\varphi}{2\pi} \left[\left(h - \frac{c}{24} \right) XY' - \frac{c}{24} XY''' \right]. \quad (2.24)$$

The analogous computation for the quantum metric is more involved, as the metric turns out to be a nonlocal functional of \mathbf{X}, \mathbf{Y} . This is due to the absolute value of m in Eq. (2.23a), which gives rise to the propagator $\sum_{m \in \mathbb{Z}} |m| e^{im(\theta-\varphi)} = -[2 \sin^2([\theta - \varphi]/2)]^{-1}$. Thus, one eventually finds

$$\mathcal{G}(\mathbf{X}, \mathbf{Y}) = \oint \frac{d\varphi d\theta}{16\pi^2} \frac{(h - \frac{c}{24})[X(\varphi) - X(\theta)][Y(\varphi) - Y(\theta)] + \frac{c}{24}[X'(\varphi) - X'(\theta)][Y'(\varphi) - Y'(\theta)]}{\sin^2([\theta - \varphi]/2)} \quad (2.25)$$

for the Virasoro quantum metric at the identity. Note how different this is from the Berry curvature (2.24), all because of the seemingly innocuous distinction between (2.23a) and (2.23b). In this sense, the Kähler structure of the parameter space (2.12) is manifest in Fourier space, but not in position space.

3 Perturbative quantum geometry

The simplest probes of quantum geometry for the coherent states (2.17) are provided by *perturbative* drives, *i.e.* deformed Hamiltonians (2.13) whose f_t is infinitesimally close to the identity. Such setups cannot probe global properties (which involve finite f_t), but do suffice to determine the quantum geometric tensor at a single point in parameter space, namely that of the undeformed Hamiltonian (2.10). Then, the key simplification is that the Lie algebra (2.9) determines everything, without involving finite conformal transformations. Homogeneity of the parameter space (2.12) further means that quantum geometry at the identity determines quantum geometry at any other point, so there is no loss of generality in focusing on infinitesimal drives as far as *local* quantum geometry is concerned.

In this section, we consider such perturbative drives to derive two universal relations: (i) the link between quantum metric and absorption rates, (ii) the link between Berry curvature and linear-response coefficients.

3.1 Virasoro quantum metric from absorption rates

Note from the quantum metric (2.21a) that the squared norm of a vector at the identity is

$$\mathcal{G}(\mathbf{X}, \mathbf{X}) = -\langle h | \mathbf{u}(\mathbf{X})^2 | h \rangle + \langle h | \mathbf{u}(\mathbf{X}) | h \rangle^2. \quad (3.1)$$

This is nothing but the variance of the Hermitian operator $i\mathbf{u}(\mathbf{X})$. Keeping in mind the fluctuation-dissipation theorem, it suggests that the quantum metric can be probed with admittance experiments. Such a proposal was indeed put forward in [52], and we apply it here to CFT.

Transition rates from perturbative Virasoro drives. Consider a time-dependent Hamiltonian (2.13) whose deformation $f_t(\varphi) = \varphi + \epsilon X_t(\varphi)$ is close to the identity in the sense that ϵ is small, while \mathbf{X}_t is some finite, time-dependent vector field that does not depend on ϵ . Then, to first order in ϵ , the perturbed Hamiltonian reads

$$H(t) = H_0 + \epsilon [\mathbf{u}(\mathbf{X}_t), H_0] + O(\epsilon^2), \quad (3.2)$$

where H_0 is the homogeneous Hamiltonian (2.10) and $\mathbf{u}(\cdot)$ is the algebra representation (2.6). We assume throughout that $X_t(\varphi)$ vanishes for $t < 0$, *i.e.* the perturbation is ‘switched on’ at $t = 0$. In the present case, we further assume that the perturbation for $t > 0$ is harmonic with frequency $\omega > 0$ so that

$$X_t(\varphi) = \begin{cases} 0 & \text{for } t < 0, \\ \frac{1}{\omega L} \cos(\omega t) X(\varphi) & \text{for } t > 0, \end{cases} \quad (3.3)$$

where $X(\varphi)$ is some dimensionless, time-independent profile. Note that the perturbation scales as $1/\omega$: the higher the frequency, the weaker the perturbation. This will turn out to be crucial for the link with the quantum metric [52].

The Hamiltonian (3.2) with \mathbf{X}_t given by Eq. (3.3) falls into the usual regime of time-dependent perturbation theory. In particular, one can perturbatively compute late-time transition rates between eigenstates of H_0 . We focus here on transitions from the highest-weight state $|h\rangle$ of Eq. (2.16) to any other eigenstate, say $|\phi\rangle$, with an energy difference $E_\phi > 0$ above that of $|h\rangle$. To leading order in ϵ , the resulting transition rate is

$$\Gamma_\phi(\omega) \sim \frac{\epsilon^2}{2\omega^2 L^2} \left| \langle \phi | [\mathbf{u}(\mathbf{X}), H_0] | h \rangle \right|^2 \delta(\omega - E_\phi) = \frac{\epsilon^2}{2L^2} \left| \langle \phi | \mathbf{u}(\mathbf{X}) | h \rangle \right|^2 \delta(\omega - E_\phi). \quad (3.4)$$

The first formula here is standard in quantum theory. The second step follows from the H_0 in the commutator and the fact that $|h\rangle$ and $|\phi\rangle$ are its eigenstates, so that the difference E_ϕ of their energies cancels against the factor $1/\omega^2$ due to the delta function.

Integrated absorption rate and quantum metric. Eq. (3.4) can be used to obtain the absorption rate induced by the perturbation (3.2) by summing over all possible final states of the transition. Since the deformed Hamiltonian (3.2) is an infinitesimal form of unitary conjugation (2.11), the only nonzero transition amplitudes are those whose final state $|\phi\rangle$ is a descendant state of $|h\rangle$, *i.e.* one that belongs to the space of the representation based on $|h\rangle$. The absorption rate thus reads

$$\Gamma(\omega) \sim \frac{\epsilon^2}{2L^2} \sum_{k=1}^{\infty} \left| \langle \phi_k | \mathbf{u}(\mathbf{X}) | h \rangle \right|^2 \delta(\omega - E_{\phi_k}), \quad (3.5)$$

where we label each descendant of $|h\rangle$ by an integer $k = 1, 2, \dots$. How exactly one chooses the labeling has no importance: the only key points are (i) that the spectrum of H_0 is discrete thanks to the finite size L , and (ii) that $|h\rangle$ is a nondegenerate eigenstate of H_0 within its irreducible representation.

Integrating the rate (3.5) over all frequencies yields

$$\int_0^\infty d\omega \Gamma(\omega) \sim \frac{\epsilon^2}{2L^2} \sum_{k=1}^\infty |\langle \phi_k | \mathbf{u}(\mathbf{X}) | h \rangle|^2 = \frac{\epsilon^2}{2L^2} \left(\langle h | \mathbf{u}(\mathbf{X}) | h \rangle^2 - \langle h | \mathbf{u}(\mathbf{X})^2 | h \rangle \right) \quad (3.6)$$

upon using that $\mathbf{u}(\cdot)$ is anti-Hermitian and writing the identity operator as $\sum_{k=1}^\infty |\phi_k\rangle\langle\phi_k| + |h\rangle\langle h|$ within the irreducible representation of $|h\rangle$. The result (3.6) manifestly involves the variance of $i\mathbf{u}(\mathbf{X})$, which we found in Eq. (3.1) to be the squared quantum norm of \mathbf{X} . In other words,

$$\int_0^\infty d\omega \Gamma(\omega) \sim \frac{\epsilon^2}{2L^2} \mathcal{G}(\mathbf{X}, \mathbf{X}) \quad (3.7)$$

where \mathcal{G} is the quantum metric at the identity coset in the infinite-dimensional parameter space (2.12). This is the result announced in Eq. (1.4). It is consistent with the protocol proposed earlier in [52], applied there to two-level systems and Bloch bands. As in [52], the same protocol can be used to measure any value $\mathcal{G}(\mathbf{X}, \mathbf{Y})$, since $\mathcal{G}(\mathbf{X}, \mathbf{Y}) = [\mathcal{G}(\mathbf{X} + \mathbf{Y}, \mathbf{X} + \mathbf{Y}) - \mathcal{G}(\mathbf{X}, \mathbf{X}) - \mathcal{G}(\mathbf{Y}, \mathbf{Y})]/2$.

3.2 Virasoro Berry curvature from linear response

Let us now link the Berry curvature (2.21b) to the linear response of the stress-energy tensor to perturbations of the form (3.2). This serves several purposes: it highlights the Kähler structure of the parameter space (2.12), it reaffirms the ballistic transport properties of CFT [24] in the language of viscosity, and it lays the foundations for the adiabatic considerations of Sec. 4. We will also briefly return to linear and nonlinear responses in Sec. 5.

Linear response to Virasoro drives. Consider again a time-dependent Hamiltonian $H(t)$ of the form (3.2), for a system prepared in the eigenstate $|h\rangle$ of H_0 at $t = 0$. In contrast to Sec. 3.1, let the vector field $\mathbf{X}_t = X_t(\varphi)\partial_\varphi$ have an arbitrary time-dependence, with modes $\hat{X}_m(t)$ in the Fourier decomposition (2.5). We are interested in the ensuing response of expectation values of Hermitian operators $i\mathbf{u}(\mathbf{Y})$ generated by the stress-energy tensor (2.6) for any vector field $\mathbf{Y} = Y(\varphi)\partial_\varphi$. Denote by $|\phi(t)\rangle$ the state at time t governed by the full time-dependent Hamiltonian. Then, standard linear-response arguments in the spirit of [60] yield (see Appendix C)

$$\langle \phi(t) | i\mathbf{u}(\mathbf{Y}) | \phi(t) \rangle = \hat{Y}_0 \left(h - \frac{c}{24} \right) + \epsilon \sum_{m,n \neq 0} \hat{Y}_m \int_0^t ds \chi_{m,n}(t, s) \hat{X}_n(s) + O(\epsilon^2) \quad (3.8)$$

with the susceptibility

$$\chi_{m,n}(t, s) \equiv \partial_s \mathcal{F}_{m,n} e^{i2\pi(mt+ns)/L} = -i \frac{2\pi}{L} m \mathcal{F}_{m,-m} e^{i2\pi m(t-s)/L} \delta_{m+n,0} \quad (3.9)$$

in terms of the Berry curvature (2.23b) in Fourier space. Formally picking $\mathbf{Y} = \delta(\varphi - \theta)\partial_\varphi$, *i.e.* the modes $\hat{Y}_m = e^{-im\theta}/2\pi$, one immediately finds

$$\langle \phi(t) | \mathcal{T}(\theta) | \phi(t) \rangle = \frac{1}{2\pi} \left(h - \frac{c}{24} \right) - \epsilon \int_0^t \frac{ds}{L} \left[\left(h - \frac{c}{24} \right) \partial_\theta^2 - \frac{c}{24} \partial_\theta^4 \right] X_s(\theta - t + s) + O(\epsilon^2) \quad (3.10)$$

for the stress-energy tensor (2.7). This amounts to rewriting Eqs. (3.8)–(3.9) in terms of the real-space, functional Berry curvature (2.24) rather than in Fourier space. Note that the zero mode of $X_t(\varphi)$ does not contribute, as was to be expected on the parameter space (2.12).

Linear response in the adiabatic regime. The perturbation $X_t(\varphi)$ is ‘adiabatic’ when each Fourier mode $\hat{X}_m(t)$ (with $m \neq 0$ without loss of generality) satisfies $L|\partial_t^{k+1}\hat{X}_m(t)| \ll |\partial_t^k\hat{X}_m(t)|$ for any $k \geq 1$. In this regime, it is meaningful to expand expectation values in time derivatives of the perturbation. Eq. (3.8) then becomes (again, see Appendix C)

$$\langle \phi(t) | i\mathbf{u}(\mathbf{Y}) | \phi(t) \rangle \sim \hat{Y}_0 \left(h - \frac{c}{24} \right) + \epsilon \sum_{m \neq 0} \mathcal{F}_{m,-m} \hat{Y}_m \left(1 + \frac{L\partial_t}{2\pi im} + O(L^2\partial_t^2/m^2) \right) \hat{X}_{-m}(t) \quad (3.11)$$

to linear order in ϵ , again involving $\mathcal{F}_{m,n}$ in Eq. (2.23b). The adiabatic version of Eq. (3.10) is

$$\langle \phi(t) | \mathcal{T}(\varphi) | \phi(t) \rangle \sim \frac{1}{2\pi} \left(h - \frac{c}{24} \right) - \frac{\epsilon}{\pi} \left(h - \frac{c}{24} - \frac{c}{24} \partial_-^2 \right) \partial_- [X_t(\varphi) - \hat{X}_0(t)] \quad (3.12)$$

in terms of the partial derivative $\partial_- \equiv \partial_\varphi - \frac{L}{2\pi}\partial_t$ along the light-cone coordinate φ^- defined above Eq. (2.1).

The links to quantum geometry are manifest, as all formulas since Eq. (3.8) involve the Berry curvature (2.23b) or its functional analogue (2.24). In the case at hand, Berry curvature and Virasoro algebra are so closely related that one can nearly read off the Virasoro commutation relations from the linear response, *e.g.* through Eq. (3.12) with the ubiquitous higher-derivative contribution of the central charge c . (Similar formulas were previously obtained in [26] for inhomogeneous CFT out of equilibrium.) Note also the similarity between Eqs. (3.11)–(3.12) and the standard definition of viscosity, where the stress-energy tensor depends on the rate of strain. Indeed, the odd viscosity of quantum Hall systems is precisely their linear response to adiabatic deformations of the metric [47]. Such deformations are implemented by unitary operators [48, 51], similar to what we did in Eq. (2.11) for CFTs. We stress, however, that the viscosity tensor vanishes in standard 1+1D CFT: its odd part is trivially zero for dimensional reasons, and its dissipative part vanishes since all perturbations propagate ballistically. Instead, our result (3.12) should be seen as a response of the thermal current to perturbations of the metric, *i.e.* a ballistic contribution to the thermal conductance of a 1+1D CFT [24, 26].

4 Quantum geometry from adiabatic drives

Having investigated perturbative probes of Virasoro quantum geometry, we now turn to finite deformations f_t in the Hamiltonian (2.13). We assume throughout that these deformations are adiabatic and periodic, with period T . Then the final state vector $|\psi(T)\rangle$ is nearly proportional to the initial one, $|\psi(0)\rangle$, and one is typically interested in their overlap,

$$\langle \psi(0) | \psi(T) \rangle. \quad (4.1)$$

To leading order in the adiabatic limit, the overlap has unit complex norm and involves a Berry phase γ_B given by the integral of the Berry connection along the curve f_t . This was studied in detail in [53], so we omit the derivation and merely state the result for later reference: given a drive f_t , the Virasoro Berry phase is⁹

$$\gamma_B[f_t] = \int_0^T \oint \frac{dt d\varphi}{2\pi} \frac{\dot{f}_t(\varphi)}{f'_t(\varphi)} \left[h - \frac{c}{24} + \frac{c}{24} \left(\frac{f''_t(\varphi)}{f'_t(\varphi)} \right)' \right] - \left(h - \frac{c}{24} \right) f_0^{-1}(f_T(0)), \quad (4.2)$$

⁹The conventions here differ from [53] by an overall sign.

where h is the highest weight introduced in (2.16) and c is the central charge. Instead, our goal here is to go beyond leading order and capture the slight misalignment between initial and final states, resulting in a nontrivial return probability given by the squared complex norm of (4.1).

Since the deformations in Eq. (2.11) are implemented by unitary operators in a representation of the group $\text{Diff}(S^1)$, the return amplitude (4.1) is intimately linked to group theory. This is also true of rotating spins and squeezed states [with groups $\text{SU}(2)$ and $\text{SL}(2, \mathbb{R})$, respectively], indeed of all generalized coherent states whose parameter space is a quotient (2.20). What follows will therefore be phrased, partly, in terms of group manifolds. While we focus for definiteness on $\text{Diff}(S^1)$, most of our arguments carry over to other groups and coherent states previously studied elsewhere, including *e.g.* [7, 61, 62].

The plan is as follows. First, we show in general terms how the Schrödinger equation with a time-dependent Hamiltonian (2.11) can be solved in terms of paths in the $\text{Diff}(S^1)$ group manifold. This expresses the return amplitude (4.1) as an expectation value in a highest-weight state, which ultimately makes it manifest that the return probability is related to the quantum metric. Second, we investigate the specific case of ‘rotating drives’ in $\text{Diff}(S^1)$. We provide an explicit formula for the resulting displacement between initial and final states, and use this to evaluate the return probability. The consequence, in all cases, is a resonance pattern similar to the one in Fig. 1.

4.1 Return amplitudes from group theory

We begin by showing how the Schrödinger equation with a time-dependent Hamiltonian (2.13) can be solved by time-dependent coherent states of the form (2.17). We then add the assumption of adiabaticity and periodicity to show that the return probability, *i.e.* the squared norm of (4.1), measures the quantum metric (3.1).

From Schrödinger to paths in a group. Let f_t be any family of deformations, and consider the time-dependent Hamiltonian $H(t) \equiv H[f_t]$ introduced in Eq. (2.13). We seek to solve the time-dependent Schrödinger equation

$$i\partial_t|\psi(t)\rangle = H(t)|\psi(t)\rangle = \mathcal{U}(f_t)H_0\mathcal{U}(f_t)^{-1}|\psi(t)\rangle \quad (4.3)$$

with an initial state $|\psi(0)\rangle = \mathcal{U}(f_0)|h\rangle$, chosen to be an eigenstate of the initial Hamiltonian. [Recall from Eq. (2.16) that $|h\rangle$ is an eigenstate of H_0 with energy $\frac{2\pi}{L}(h - \frac{c}{24})$.] The strategy is to reformulate the Schrödinger equation (4.3) as an equation of motion in the group manifold by stripping off information about the Hilbert space and the representation \mathcal{U} . To this end, make the ansatz

$$|\psi(t)\rangle = e^{i\alpha_t} \mathcal{U}(g_t)|h\rangle, \quad (4.4)$$

where $\alpha_t \in \mathbb{R}$ is a time-dependent overall phase (such that $\alpha_0 = 0$) and $g_t \in \text{Diff}(S^1)$ is a path in the group manifold (such that $g_0 = f_0$). Both sides of Eq. (4.3) then take the form of operators acting on the highest-weight state $|h\rangle$. Thus, Eq. (4.3) certainly holds if the operators themselves are equal, *i.e.* if

$$-\partial_t\alpha_t + i[\partial_t \mathcal{U}(g_t)] \mathcal{U}(g_t)^{-1} = \mathcal{U}(f_t)H_0\mathcal{U}(f_t)^{-1}. \quad (4.5)$$

The right-hand side can be made more explicit thanks to the fact that H_0 itself is a Lie algebra generator. Indeed, we already computed it in Eq. (2.15). For later convenience, we now write

it as $\mathcal{U}(f_t)H_0\mathcal{U}(f_t)^{-1} = \frac{2\pi i}{L}\mathbf{u}(\mathbf{V}_t) + C[f_t]$, where

$$\mathbf{V}_t \equiv V_t(\varphi)\partial_\varphi \equiv \frac{\partial_\varphi}{(f_t^{-1})'(\varphi)} \quad (4.6)$$

is a time-dependent vector field. Note that $V_t(\varphi)$ is essentially the dimensionless velocity profile introduced in Eq. (1.1): one has $V_t(\varphi) = v_t(x)$ for $\varphi = 2\pi x/L$.

This is the point where information is needed on the operators $\mathcal{U}(g)$. As stated in Eq. (2.3), they furnish a projective representation of $\text{Diff}(S^1)$, so the left-hand side of Eq. (4.5) involves $[\partial_t \mathcal{U}(g_t)]\mathcal{U}(g_t)^{-1} = \mathbf{u}(\dot{g}_t \circ g_t^{-1}) + ic\partial_s \mathbf{C}(g_s, g_t^{-1})|_{s=t}$, where $\dot{g}_t \equiv \partial_t g_t$ and $\mathbf{C}(\cdot, \cdot)$ is the Bott cocycle (2.4). We get rid of all terms proportional to the central charge c by choosing the time-dependent phase α_t such that

$$-\partial_t \alpha_t - c\partial_s \mathbf{C}(g_s, g_t^{-1})|_{s=t} = C[f_t], \quad (4.7)$$

so what remains of Eq. (4.5) is $\mathbf{u}(\dot{g}_t \circ g_t^{-1}) = \frac{2\pi}{L}\mathbf{u}(\mathbf{V}_t)$. This, in turn, is satisfied if

$$\dot{g}_t \circ g_t^{-1} = \frac{2\pi}{L}\mathbf{V}_t, \quad (4.8)$$

which was the desired result: it is an equation for the time-dependent diffeomorphism g_t that no longer makes any reference to a Hilbert space or operators thereon. If Eqs. (4.8) and (4.7) hold, then so does the Schrödinger equation (4.3) with the ansatz (4.4).

A straightforward analogue of Eq. (4.8) holds in other situations involving generalized coherent states when the Hamiltonian preserves coherence [*i.e.* when $H(t) = i\mathbf{u}(\mathbf{V}_t)$ for some Lie algebra element \mathbf{V}_t]. The only difference lies in the choice of group manifold; see *e.g.* [63, 64] for the case of squeezed states. For $G = \text{Diff}(S^1)$ as in our current setup, Eq. (4.8) admits a hydrodynamical interpretation: \mathbf{V}_t can be seen as a time-dependent vector field that determines the local velocity of a (compressible) fluid on S^1 , and the solution $g_t(\varphi)$ of Eq. (4.8) gives the time-dependent position of a fluid parcel initially located at $g_0(\varphi) = f_0(\varphi)$. Equivalently, g_t is the one-parameter flow generated by \mathbf{V}_t (with respect to the dimensionless time $2\pi t/L$).

Return probability and quantum metric. Let us now add two assumptions, namely (i) that the velocity vector field \mathbf{V}_t is periodic in time with period T , and (ii) that its time dependence is slow, or adiabatic, in the sense that the operator norm of $\partial_t H(t)$ is much smaller than $1/L^2$. In that limit, the adiabatic theorem states that the solution (4.4) sticks closely to $\mathcal{U}(f_t)|h\rangle$, up to a time-dependent phase [65]. Put differently, the coset of g_t on the parameter space (2.20) coincides with that of f_t . The return amplitude (4.1) is thus a pure phase to leading order, involving in particular a Berry phase. As the latter is studied in detail in [53], we do not dwell on it here. Our focus is instead on the first subleading correction to the adiabatic theorem, which accounts for a small difference between the cosets of g_t and f_t on the parameter space (2.20); see Fig. 4. This leads to a nontrivial return probability given by the square of the amplitude (4.1).

To be specific, let $0 < \delta \ll 1$ denote a dimensionless adiabatic parameter, with $\delta \rightarrow 0$ indicating the adiabatic limit. The small displacement between the cosets $g_t G_0$ and $f_t G_0$ in the parameter space (2.20) can be represented by a time-dependent Lie algebra element \mathbf{Y}_t defined as follows: at each time t , there exists a finite rotation $R_{\theta(t)}(\varphi) = \varphi + \theta(t)$ by an angle $\theta(t)$ such that

$$f_t^{-1} \circ g_t = R_{\theta(t)} \circ e^{\delta \mathbf{Y}_t}, \quad (4.9)$$

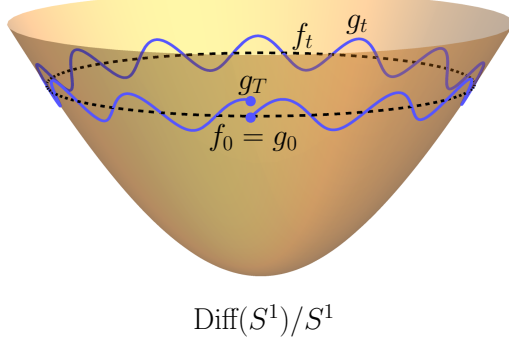


Figure 4: Cartoon of the parameter space (2.12), showing the periodic drive f_t and the corresponding solution g_t of Eq. (4.8). In the adiabatic limit, the cosets $f_t G_0$ and $g_t G_0$ nearly coincide, but not quite, due to the small micromotion of g_t . Their mismatch ultimately causes a nontrivial overlap $|\langle \psi(0) | \psi(T) \rangle| = |\langle h | \mathcal{U}(g_0)^{-1} \mathcal{U}(g_T) | h \rangle| \neq 1$ that essentially measures the quantum distance between nearby Gaussian wave functions. See also Fig. 5 below.

where \mathbf{Y}_t is finite at all times in the adiabatic limit $\delta \rightarrow 0$. [Rotations appear here because they span the stabilizer of the undeformed Hamiltonian (2.10).] Using this in the ansatz (4.4), the return amplitude (4.1) can be adiabatically expanded in $\delta \ll 1$ as

$$\langle \psi(0) | \psi(T) \rangle = e^{i\alpha_T + i\mathcal{C}(f_0^{-1}, g_T)} \langle h | \mathcal{U}(f_0^{-1} \circ g_T) | h \rangle \quad (4.10)$$

$$= e^{i\Theta} \left(1 - \frac{\delta^2}{2} \left[\langle h | [i\mathbf{u}(\mathbf{Y}_T)]^2 | h \rangle - \langle h | i\mathbf{u}(\mathbf{Y}_T) | h \rangle^2 \right] \right) + O(\delta^3), \quad (4.11)$$

where Θ is a complicated overall phase—the sum of a dynamical phase and a Berry phase (4.2), plus subleading corrections in $L/T \sim \delta$. For our purposes, the key part of Eq. (4.11) is the one that is *not* a phase, giving rise to the return probability [7]

$$|\langle \psi(0) | \psi(T) \rangle|^2 \sim 1 - \delta^2 \left(\langle h | [i\mathbf{u}(\mathbf{Y}_T)]^2 | h \rangle - \langle h | i\mathbf{u}(\mathbf{Y}_T) | h \rangle^2 \right) = 1 - \delta^2 \mathcal{G}(\mathbf{Y}_T, \mathbf{Y}_T). \quad (4.12)$$

Here one recognizes the quantum metric (3.1), yielding the squared norm of \mathbf{Y}_T .¹⁰ Note that this is the metric at the identity, even though it measures the distance between the rays of $\mathcal{U}(g_T) | h \rangle$ and $\mathcal{U}(g_0) | h \rangle$, with g_T and g_0 both well away from the identity. This is again because the parameter space (2.20) is homogeneous, *i.e.* quantum geometry at the identity determines quantum geometry everywhere.

4.2 Return probabilities for rotating drives

We call *rotating drive* a family of time-dependent deformations given by

$$f_t(\varphi) = f_0(\varphi) + \omega t \quad (4.13)$$

where $\omega \equiv 2\pi/T > 0$ is some frequency and $f_0 \in \text{Diff}(S^1)$ is a given, fixed transformation. Any such family of deformations gives rise to a periodic Hamiltonian (2.13). Our goal is to find the resulting return probability (4.12) in the adiabatic limit $\omega L \rightarrow 0$, where L is system size. We do this by first solving Eq. (4.8), which turns out to be integrable in the case of rotating drives. We then find the vector field \mathbf{Y}_t in the group element (4.9), deduce the overlap $|\langle h | \mathcal{U}(f_t^{-1} g_t) | h \rangle|^2$ at all times, and read off the return probability after one cycle.

¹⁰More precisely, the squared norm of $\mathbf{Y}_T + \mathbf{g}_0$, seen as a tangent vector of the manifold (2.20) at the identity. What we call \mathbf{Y}_T here was called \mathbf{Y} in Eq. (1.6).

Motion in parameter space for rotating drives. For rotating drives (4.13), the right-hand side of Eq. (4.8) is a vector field with profile $V_t(\varphi) = V_0(\varphi - \omega t)$, where $V_0(\varphi) = 1/(f_0^{-1})'(\varphi)$ owing to Eq. (4.6). It is a local velocity that rotates around the circle at constant angular velocity ω . The corresponding flow g_t is readily found with the same ansatz as in [66, 67]: denoting by $R_\theta(\varphi) \equiv \varphi + \theta$ the rotation by θ , let

$$g_t = R_{\omega t} \circ \zeta \circ R_{\Omega t} \circ \zeta^{-1} \circ g_0, \quad (4.14)$$

where the two unknowns are the deformation $\zeta \in \text{Diff}(S^1)$ and the angular velocity Ω , both time-independent. The initial condition g_0 is arbitrary; choosing $g_0 = f_0$ ensures that the initial state $|\psi(0)\rangle = \mathcal{U}(f_0)|h\rangle$ is an eigenstate of the initial Hamiltonian, as in Sec. 4.1. Plugging the ansatz (4.14) into Eq. (4.8) and using the winding condition (2.2) yields

$$(\zeta^{-1})'(\varphi) = \frac{\Omega}{\frac{2\pi}{L}V_0(\varphi) - \omega}, \quad \frac{1}{\Omega} = \frac{1}{2\pi} \oint \frac{d\varphi}{\frac{2\pi}{L}V_0(\varphi) - \omega}, \quad (4.15)$$

which entirely determines the flow (4.14).¹¹ Note that this is only well-defined if $V_0(\varphi) - \frac{\omega L}{2\pi}$ never vanishes on the circle; in the adiabatic limit $\omega L \rightarrow 0$, this amounts to requiring that $V_0(\varphi)$ never vanishes, which is indeed satisfied by any velocity profile of the form (4.6).

Having found g_t , it is now straightforward to write the group element whose expectation value yields the return amplitude (4.10). With the initial condition $g_0 = f_0$, Eq. (4.14) yields

$$f_0^{-1} \circ g_T = f_0^{-1} \circ \zeta \circ R_{\Omega T} \circ \zeta^{-1} \circ f_0. \quad (4.16)$$

This deformation is generally complicated—it is well away from the identity in $\text{Diff}(S^1)$ —but we are specifically interested in the adiabatic regime $\omega L \ll 1$ where things simplify. To quickly see why, expand Eqs. (4.15) in the adiabatic limit and keep only the leading term, which yields $\Omega \sim 2\pi/L$ and $(\zeta^{-1})'(\varphi) \sim 1/V_0(\varphi) = (f_0^{-1})'(\varphi)$. Thus, $\zeta \sim f_0$ in the adiabatic limit, so Eq. (4.14) implies $\lim_{\omega L \rightarrow 0} g_t = f_t \circ R_{2\pi t/L}$ and the group element (4.16) boils down to a pure rotation $f_0^{-1} \circ g_T \sim R_{2\pi T/L}$. The latter gives rise to the expected dynamical phase in the amplitude (4.10). Our goal is to go beyond leading order by finding the small deviation of Eq. (4.16) away from a rotation.

Adiabatic expansion. Since $\Omega \sim 2\pi/L$ in the adiabatic limit, let us set up the adiabatic expansion by defining the ‘effective’ adiabatic parameter

$$\delta \equiv \frac{\omega}{\Omega} = \frac{1}{2\pi} \oint \frac{(L/T) d\varphi}{V_0(\varphi) - L/T} \ll 1, \quad (4.17)$$

where Ω was defined in Eq. (4.15). This can be contrasted with the ‘bare’ adiabatic parameter $\omega L/2\pi = L/T$. The two are related by the adiabatic expansion of Eq. (4.15), namely

$$\frac{1}{\delta} = \frac{T}{L} - \oint \frac{d\varphi}{2\pi f_0'(\varphi)} - \frac{L}{T} \left[\oint \frac{d\varphi}{2\pi f_0'(\varphi)^2} - \left(\oint \frac{d\varphi}{2\pi f_0'(\varphi)} \right)^2 \right] + O\left(\frac{L^2}{T^2}\right), \quad (4.18)$$

confirming that $\delta \sim L/T$ to leading order. In practice, the first two terms of the expansion (4.18) often suffice. They are reminiscent of a dynamical phase and a Berry phase, to which they will be seen to correspond for $\text{SL}(2, \mathbb{R})$ drives in Sec. 5.

¹¹This also shows that the ansatz (4.14) indeed is the solution of Eq. (4.8) for rotating drives.

It remains to compute the deformation $\zeta^{-1} \circ f_0$ of Eq. (4.16). The latter is close to the identity in the adiabatic limit: the expansion of Eq. (4.15) in powers of L/T yields

$$\zeta^{-1}(f_0(\varphi)) = \varphi + \delta Z(\varphi) + O(\delta^2), \quad Z(\varphi) \equiv \int_0^\varphi d\alpha \left(\frac{1}{f'_0(\alpha)} - \oint \frac{d\theta}{2\pi f'_0(\theta)} \right), \quad (4.19)$$

where we used Eq. (4.18) to trade L/T for δ . As expected, this is an infinitesimal diffeomorphism involving a vector field $\delta Z(\varphi)\partial_\varphi$. One can now plug $\zeta^{-1} \circ f_0$ into Eq. (4.14) with $g_0 = f_0$ to find

$$f_t^{-1}(g_t(\varphi)) = \varphi + \Omega t + \delta Y_t(\varphi) + O(\delta^2) \quad \text{with} \quad Y_t(\varphi) \equiv Z(\varphi) - Z(\varphi + \Omega t). \quad (4.20)$$

This is indeed a diffeomorphism of the form identified in Eq. (4.9), with a rotation by $\theta(t) = \Omega t$ and a small $O(\delta)$ correction involving the time-dependent vector field $\mathbf{Y}_t = Y_t(\varphi)\partial_\varphi$. The latter can be expressed in terms of $f_0(\varphi)$ thanks to Eq. (4.19). Note that this holds at all times; at the end of one cycle, one has $\Omega t = \Omega T = 2\pi/\delta$ in terms of the adiabatic parameter (4.17).

Return probabilities. The return probability (4.12) is entirely determined by the Lie algebra element \mathbf{Y}_T , which we have just found in Eqs. (4.19)–(4.20). Using the quantum metric written in Eq. (2.25), we conclude that

$$\begin{aligned} |\langle \psi(0) | \psi(T) \rangle|^2 \sim 1 - \delta^2 \oint \frac{d\varphi d\theta}{16\pi^2 \sin^2([\varphi - \theta]/2)} & \left(\left(h - \frac{c}{24} \right) \left[\int_\theta^{\theta + \frac{2\pi}{\delta}} \frac{d\alpha}{f'_0(\alpha)} - \int_\varphi^{\varphi + \frac{2\pi}{\delta}} \frac{d\alpha}{f'_0(\alpha)} \right]^2 \right. \\ & \left. + \frac{c}{24} \left[\frac{1}{f'_0(\theta + \frac{2\pi}{\delta})} - \frac{1}{f'_0(\theta)} - \frac{1}{f'_0(\varphi + \frac{2\pi}{\delta})} + \frac{1}{f'_0(\varphi)} \right]^2 \right) \end{aligned} \quad (4.21)$$

for adiabatic rotating drives in CFT, where we used $\Omega T = 2\pi/\delta$. This is plotted in Fig. 1 as a function of $T/L \sim 1/\delta$ for different choices of the initial deformation f_0 .

A striking aspect of the plots in Fig. 1 is the oscillating convergence of the return probability in the adiabatic limit $T/L \rightarrow \infty$. These oscillations stem from the ubiquitous appearance, in Eq. (4.21), of the shift by $2\pi/\delta \sim T/L$ in the 2π -periodic function $1/f'_0(\varphi)$: depending on the value of $2\pi/\delta$, the shift gives rise to constructive or destructive ‘interferences’ of $1/f'_0(\varphi)$. A more direct way to predict such oscillations is to refer to the expression (2.22a) of the Virasoro quantum metric in terms of Fourier modes. In the case at hand, the Fourier modes of $Y_t(\varphi)$ in Eq. (4.19) are $\hat{Y}_m(t) = \hat{Z}_m(1 - e^{im\Omega t})$, where \hat{Z}_m is the m^{th} mode of $1/f'_0(\varphi)$ (for $m \neq 0$). The exponential $e^{im\Omega t}$ leads to an oscillating pattern of the squared quantum norm

$$\mathcal{G}(\mathbf{Y}_t, \mathbf{Y}_t) = 4 \sum_{m \in \mathbb{Z}} |m| \left(h + \frac{c}{24} (m^2 - 1) \right) |\hat{Z}_m|^2 \sin^2(m\Omega t/2) \quad (4.22)$$

as a function of t , reflecting the micromotion of g_t around f_t visible in Fig. 4. This micromotion is manifest in the time-dependent overlap $|\langle h | \mathcal{U}(f_t^{-1} \circ g_t) | h \rangle|^2 \sim 1 - \delta^2 \mathcal{G}(\mathbf{Y}_t, \mathbf{Y}_t)$ between the exact state $\propto \mathcal{U}(g_t) |h\rangle$ and its adiabatic approximation $\propto \mathcal{U}(f_t \circ R_{2\pi t/L}) |h\rangle$.

5 Rotating drives in $\text{SL}(2, \mathbb{R})$

The simplest inhomogeneous Hamiltonians (1.1) have a velocity profile involving a single wavenumber k , so that $v_t(x) = A_t + B_t \cos(2\pi kx/L - C_t)$ with generally time-dependent coefficients $A_t > |B_t|$, B_t , and C_t . In contrast to the protocols of Secs. 3 and 4, such drives do not

probe the full parameter space of conformal frames. They are limited, instead, to the subgroup of $\text{Diff}(S^1)$ that consists of transformations of the form

$$e^{ikf(\varphi)} = \frac{\alpha e^{ik\varphi} + \beta}{\bar{\beta} e^{ik\varphi} + \bar{\alpha}} \quad (5.1)$$

where $\alpha, \beta \in \mathbb{C}$ satisfy $|\alpha|^2 - |\beta|^2 = 1$. This subgroup is finite-dimensional and locally isomorphic to $\text{SL}(2, \mathbb{R}) \cong \text{SU}(1, 1)$. As a result, the dynamics of coherent states can be wholly expressed in terms of finite-dimensional matrices. We now study one such situation with a rotating drive $v_t(x) = A + B \cos(2\pi kx/L - \omega t)$ (where $A > |B|$ and B are constants) and show that the evolution operator can be computed *exactly* for any driving frequency $\omega > 0$ and general amplitudes A, B . This, in turn, allows us to compute nonlinear responses and return amplitudes in any driving regime, as illustrated in Fig. 3.

5.1 Evolution operator

Pick an integer wavenumber k and a real ‘rapidity’ parameter $\lambda > 0$. Given the CFT stress-energy tensor $\mathcal{T}(\varphi)$, consider the time-dependent inhomogeneous Hamiltonian

$$H(t) = \frac{2\pi}{L} \oint d\varphi \left[\cosh(2\lambda) - \sinh(2\lambda) \cos(k[\varphi - \omega t]) \right] \mathcal{T}(\varphi) + \frac{\pi c}{12L} [\cosh(2\lambda) - 1]. \quad (5.2)$$

This takes the form (2.15) for a rotating drive (4.13) whose ‘initial deformation’ f_0 is given by Eq. (5.1) with $\alpha = \cosh(\lambda)$ and $\beta = \sinh(\lambda)$. Equivalently, one has

$$H(t) = \frac{2\pi}{L} \left[\cosh(2\lambda) L_0 - \frac{1}{2} \sinh(2\lambda) \left(e^{ik\omega t} L_k + e^{-ik\omega t} L_{-k} \right) \right] + \frac{\pi c}{12L} [(k^2 - 1) \cosh(2\lambda) - 1] \quad (5.3)$$

in terms of the Virasoro generators introduced in Eq. (2.7). The Hamiltonian thus involves only $\{L_{-k}, L_0, L_k\}$, which generate an $\mathfrak{sl}(2, \mathbb{R}) \cong \mathfrak{su}(1, 1)$ subalgebra (see Appendix D). It follows that the evolution operator

$$U(t) \equiv \overleftarrow{\mathcal{T}} \exp \left(-i \int_0^t dt' H(t') \right), \quad (5.4)$$

with ordering $\overleftarrow{\mathcal{T}}$ so that time increases from right to left, belongs to the corresponding $\text{SL}(2, \mathbb{R}) \cong \text{SU}(1, 1)$ subgroup of $\text{Diff}(S^1)$. Since this is a matrix group, one may hope to use matrix multiplication to compute $U(t)$, despite the nontrivial time ordering $\overleftarrow{\mathcal{T}}$. No such simplification would be available in the full Virasoro algebra.

To obtain the evolution operator (5.4), we write the time-ordered exponential as

$$U(t) = \lim_{M \rightarrow \infty} \overleftarrow{\prod}_{m=0, \dots, M} e^{-iH(m\delta t)\delta t}, \quad (5.5)$$

where $\delta t \equiv t/M$ and the product $\overleftarrow{\prod}$ is ordered so that time increases from right to left. Each factor in this product can be viewed as (a unitary representation of) a matrix in $\text{SU}(1, 1)$. Thus, one may just as well deal with the matrices directly, and evaluate their product. This is explained in Appendix D, to which we refer for details. Suffice it to say that a key simplification occurs thanks to the drive being a rotating one, in the sense of Eq. (4.13): the m dependence of

each factor in (5.5) cancels out against the $(m + 1)$ of the next factor, and the entire evolution operator (5.5) becomes the M^{th} power of a time-independent matrix. The end result is

$$U(t) = e^{-i\frac{\pi c}{12L}k^2t[\cosh(2\lambda)-1]}e^{-i\omega t(L_0-c/24)}e^{-i\frac{2\pi}{L}t\left([\cosh(2\lambda)-L/T](L_0-c/24)-\sinh(2\lambda)\frac{L-k+L_k}{2}\right)}, \quad (5.6)$$

expressed in terms of the Virasoro generators. Note the structure of this expression, which is consistent with the evolution operator for coherent states in Eq. (4.4) and the specific form (4.14) of g_t for rotating drives. Indeed, using $e^{i\alpha t}\mathcal{U}(g_t) = U(T)\mathcal{U}(g_0)$, one can identify the second exponential in Eq. (5.6) with the undeformed rotation $R_{\omega t}$, while the last exponential in Eq. (5.6) can be shown to represent the ‘deformed rotation’ $\zeta \circ R_{\Omega t} \circ \zeta^{-1}$. In the case at hand, ζ is an $\text{SU}(1,1)$ deformation of the form (5.1) with (see again Appendix D)

$$\alpha = \frac{1 + \Lambda}{2\sqrt{\Lambda}}, \quad \beta = \frac{1 - \Lambda}{2\sqrt{\Lambda}}, \quad \Lambda \equiv 2\pi \frac{e^{-2\lambda} - L/T}{L\Omega}, \quad (5.7)$$

and the frequency of the rotation is

$$\Omega = \frac{2\pi}{L} \sqrt{1 - 2 \cosh(2\lambda)(L/T) + (L/T)^2}, \quad (5.8)$$

all of which is consistent with Eq. (4.15). What is special about $\text{SL}(2, \mathbb{R})$ drives is that the deformed rotation can be written as an explicit exponential of finitely many Virasoro generators. This would not be true with more general rotating drives, as we saw in Sec. 4.

Motion on parameter space. Since the solution (4.4) of the Schrödinger equation consists of coherent states, the dynamics encoded by the evolution operator (5.6) defines a path in the parameter space (2.20): at time t , the state vector $|\psi(t)\rangle = e^{i\alpha t}\mathcal{U}(g_t)|h\rangle$ defines a unique coset $g_t G_0 \in G/G_0$. (Conversely, the coset $g_t G_0$ uniquely determines the ray $[\psi(t)] = [\mathcal{U}(g_t)|h\rangle]$.) The situation is especially simple for $\text{SL}(2, \mathbb{R})$ drives, which only involve three Virasoro generators $\{L_{-k}, L_0, L_k\}$ and therefore probe a two-dimensional parameter space $\text{SL}(2, \mathbb{R})/S^1$ (*i.e.* a hyperbolic plane). One can thus view the motion of the ray $[\psi(t)]$ as a curve on a hyperbolic disk, as in Fig. 5. Concretely, the curve is obtained by writing the ray of the state vector as

$$[\psi(t)] = [e^{\chi_t L_{-k} - \bar{\chi}_t L_k} |h\rangle] \quad (5.9)$$

where χ_t is a time-dependent complex number that can be conveniently parametrized as $\chi_t \equiv \frac{1}{k} \text{artanh}(|\eta_t|) \frac{\eta_t}{|\eta_t|}$ in terms of η_t on the unit (Poincaré) disk. One finds (see Appendix D)

$$\eta_t \equiv \tanh(k|\chi_t|) \frac{\chi_t}{|\chi_t|} = \tanh(\lambda) \frac{1 + i\left(\frac{2\pi}{L\Omega} + \frac{\omega}{\Omega}\right) \tan(k\Omega t/2)}{1 + i\left(\frac{2\pi}{L\Omega} - \frac{\omega}{\Omega}\right) \tan(k\Omega t/2)} e^{-ik\omega t} \quad (5.10)$$

with Ω the frequency in Eq. (5.8). This is illustrated in Fig. 5. Note the behavior in the adiabatic limit, where $\lim_{L/T \rightarrow 0} \eta_t = \tanh(\lambda) e^{-ik\omega t}$ essentially coincides with the rotating drive, as was to be expected. In fact, the complex variable η_t is known to satisfy a Riccati equation with time-dependent coefficients determined by the external drive [63], but this perspective is not needed in our case.

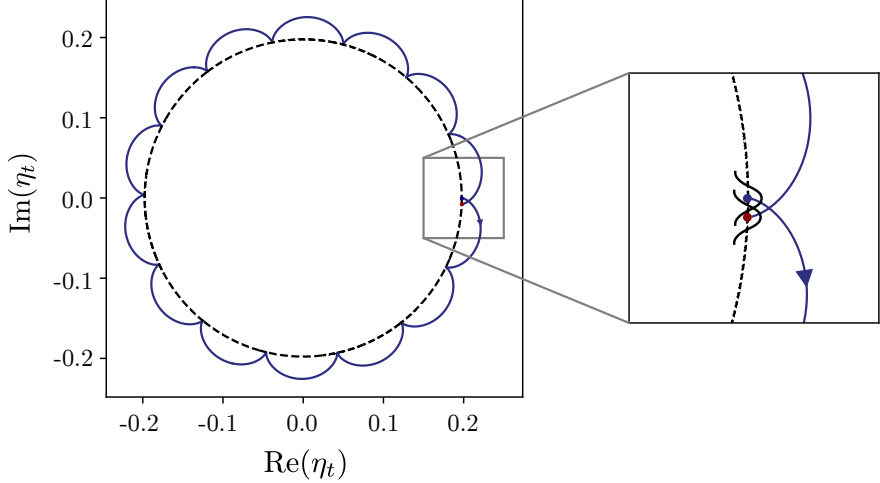


Figure 5: Time evolution of the unit disk coordinate η_t in Eq. (5.10) induced by the dynamics given by the Hamiltonian (5.3) with $k = 1$ and $\lambda = 0.2$. The result $\tanh(\lambda)e^{-ik\omega t}$ in the adiabatic limit $L/T \rightarrow 0$ for the trajectory η_t is shown as a black dashed line, while the blue curve shows the nonadiabatic result for $L/T = 1/15$. After one full period, the final state (red dot) does not exactly return to the initial state (blue dot). The slight mismatch between the corresponding wave functions (coherent states) gives rise to a nearly saturated return probability.

5.2 Nonlinear and linear responses

A first application of the evolution operator (5.6) is to compute the effect of the driven Hamiltonian (5.2) on any operator (2.6) generated by the stress-energy tensor, similarly to what we did in Sec. 3 to linear order. The result is actually quite general: provided g_t is chosen such that the state vector $|\phi(t)\rangle = e^{i\alpha_t} \mathcal{U}(g_t)|h\rangle$ solves the Schrödinger equation (4.3) with initial condition $|\phi(0)\rangle = \mathcal{U}(g_0)|h\rangle$, the corresponding expectation value of $i\mathbf{u}(\mathbf{Y})$ is

$$\langle \phi(t) | i\mathbf{u}(\mathbf{Y}) | \phi(t) \rangle = \frac{1}{2\pi} \oint d\varphi Y(\varphi) \left(\left(h - \frac{c}{24} \right) [(g_t^{-1})'(\varphi)]^2 - \frac{c}{12} \{g_t^{-1}(\varphi), \varphi\} \right). \quad (5.11)$$

This readily follows from the transformation law (2.14) of the CFT stress tensor, and it holds regardless of the initial g_0 . In the case of rotating drives, Eq. (4.14) allows one to express $\langle \phi(t) | i\mathbf{u}(\mathbf{Y}) | \phi(t) \rangle$ in terms of the deformation $\zeta(\varphi)$, the frequency Ω , and g_0 .

For the specific case of rotating drives in $SL(2, \mathbb{R})$, this gives explicit access to the full nonlinear response. Indeed, $\zeta(\varphi)$ is explicitly known to be of the form (5.1) with α, β in Eq. (5.7), and Ω is also known exactly from Eq. (5.8). Choosing g_0 to be the identity, and considering the special case of small perturbations, *i.e.* when $\epsilon = \lambda$ is small, it follows that

$$\langle \phi(t) | \mathcal{O} | \phi(t) \rangle = \left(h - \frac{c}{24} \right) \hat{Y}_0 - i\epsilon \mathcal{F}_{k,-k} \left(\hat{Y}_k \frac{e^{ik\omega t} - e^{ik2\pi t/L}}{k(1 - L/T)} + \hat{Y}_{-k} \frac{e^{-ik\omega t} - e^{-ik2\pi t/L}}{k(1 - L/T)} \right) + O(\epsilon^2) \quad (5.12)$$

in terms of the Berry curvature $\mathcal{F}_{m,n}$ of Eq. (2.23b). This agrees with the general linear-response result (3.8)–(3.9) by noting that the \mathbf{X}_t in Eq. (3.2) is now given by $X_t(\varphi) = -\frac{2}{k} \sin(k[\varphi - \omega t])$. In fact, the general expression (5.11) is consistent with our linear-response formulas (3.8)–(3.9): this can be shown by expressing $g_t(\varphi)$ in terms of a weakly perturbed $f_t(\varphi) = \varphi + \epsilon X_t(\varphi)$.

5.3 Return amplitudes and probabilities

A second application of the evolution operator (5.6) is to yield the solution $U(t)|\psi(0)\rangle$ of the Schrödinger equation (4.3) for any initial condition $|\psi(0)\rangle$. As in Sec. 4, we choose $|\psi(0)\rangle = \mathcal{U}(f_0)|h\rangle$ to be an eigenstate of the initial inhomogeneous Hamiltonian, and investigate the return amplitude (4.1). This can again be done in terms of 2×2 matrices, and the return amplitude can in fact be evaluated for any time t (as opposed to $t = T$ at the end of one cycle). In terms of the convenient parameter $h_k \equiv h + \frac{c}{24}(k^2 - 1)$, one finds (see Appendix D)

$$\langle\psi(0)|\psi(t)\rangle = e^{i\pi ck^2 t/12L} u_t^{-2h_k/k} \quad (5.13)$$

with

$$\begin{aligned} u_t = & \cos(k\Omega t/2) \cos(k\omega t/2) - 2\pi \frac{\cosh(2\lambda) - L/T}{L\Omega} \sin(k\Omega t/2) \sin(k\omega t/2) \\ & + i \cosh(2\lambda) \left[\cos(k\Omega t/2) \sin(k\omega t/2) + 2\pi \frac{\operatorname{sech}(2\lambda) - L/T}{L\Omega} \sin(k\Omega t/2) \cos(k\omega t/2) \right] \end{aligned} \quad (5.14)$$

expressed in terms of the frequency Ω in Eq. (5.8). The overall phase of $\langle\psi(0)|\psi(t)\rangle$ can be extracted by picking the branch of $\arg(u_t)$ consistent with the limiting case $\lambda = 0$, for which the phase is purely dynamical. This generalizes previous results for the return probability in $\mathfrak{sl}(2, \mathbb{R})$ -driven CFT [68], which were restricted to piecewise-constant time-dependent Hamiltonians. Furthermore, the return probability was recently studied for continuous Floquet drives in [69], which relied on Floquet perturbation theory, while the result (5.13) is exact and uses no perturbation theory.

As before, one is most interested in the return amplitude (4.1) after one period, in the adiabatic limit $L/T \rightarrow 0$. Taking $t = T$ in Eq. (5.13) and expanding (5.14) in that limit yields

$$\langle\psi(0)|\psi(T)\rangle = \exp \left[2\pi i \left(-h_0 \frac{T}{L} + h_k [\cosh(2\lambda) - 1] + h_k \frac{\sinh^2(2\lambda)}{2} \frac{L}{T} \right) \right] \left[1 + O(L^2/T^2) \right] \quad (5.15)$$

where the exponent manifestly involves a dynamical phase and a Berry phase, plus a first nonadiabatic correction. The Berry phase, in particular, is consistent with Eq. (4.2) for a rotating drive in $\operatorname{SL}(2, \mathbb{R})$ [53].

Note that the return amplitude (5.15) has unit norm up to L^2/T^2 corrections, so it is those corrections that are responsible for the nontrivial return probability $|\langle\psi(0)|\psi(T)\rangle|^2$. As in Sec. 4, the corrections are most conveniently found by expanding in powers of the adiabatic parameter (4.17) rather than L/T . One finds

$$|\langle\psi(0)|\psi(T)\rangle|^2 = 1 - \delta^2 \frac{2h_k}{k} \sinh^2(2\lambda) \sin^2(\pi k/\delta) + O(\delta^3), \quad (5.16)$$

which shows that there is an oscillating tail in the return probability beyond the adiabatic limit, as in Fig. 6. This result is a special case of the general adiabatic expansion (4.21). A single Fourier mode k now appears in the quantum metric (4.22), since in fact the vector field $\mathbf{Y}_t = Y_t(\varphi)\partial_\varphi$ of Eq. (4.20) is now explicitly given by $Y_t(\varphi) = \sinh(2\lambda)[\sin(k\varphi) - \sin(k[\varphi + \Omega t])]$. The oscillations of Eq. (5.16) with T can then be understood by referring to Fig. 5: the micromotion around the leading adiabatic approximation has a (high) frequency Ω of its own, which may or may not resonate with the (low) frequency ω of the drive. At resonance, when $\Omega T \in 2\pi\mathbb{Z}$, the initial and final rays coincide.

In Fig. 6, we also plot the corresponding result for a periodic free-fermion chain at half filling with N sites and driven, inhomogeneous nearest-neighbor couplings of the form

$$J_j(t) = \cosh(2\lambda) - \sinh(2\lambda) \cos(k(2\pi j/N - \omega t)). \quad (5.17)$$

The return probability $|\langle \psi_N(0) | \psi_N(T) \rangle|^2$ of the lattice quantum state is computed numerically by approximating the evolution operator with a finite number of steps and using exact diagonalization for each time step; see Appendix E. The result exhibits remarkable agreement with the analytical formula that can be deduced from the square of Eq. (5.13). This is true even far away from the adiabatic regime, as long as the strength of the perturbation (controlled by λ) is sufficiently weak. Importantly, CFT results for the return probability are even applicable to lattice systems with a relatively small number of lattice sites, as shown in Fig. 6(b). This suggests that our dynamical probes for quantum geometry could potentially be implemented in quantum simulators with fewer than a hundred sites.

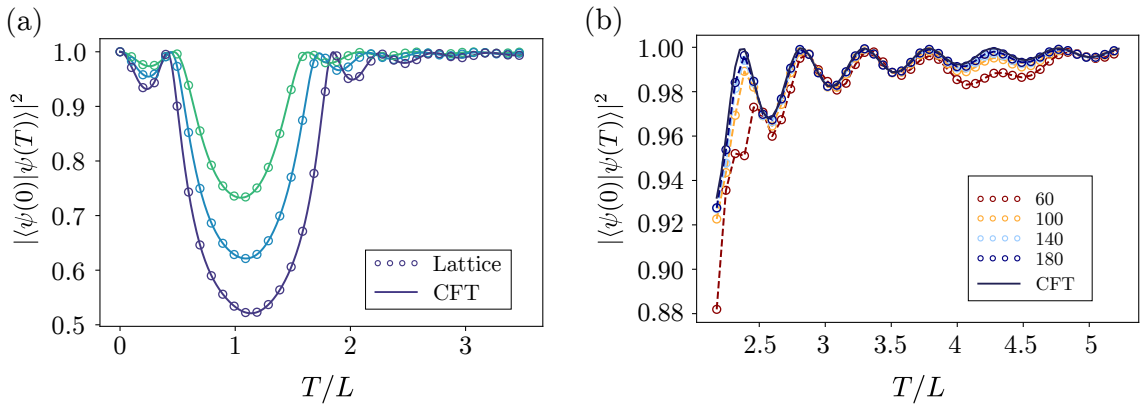


Figure 6: (a) Return probability after time evolving under the Hamiltonian (5.3) for one full cycle. The results are plotted as a function of T/L for $\lambda = 0.15, 0.2, 0.25$ (green to purple). [The parameters are $L = 200$, $k = 2$, $c = 1$, $h = 0$ and periodic boundary conditions are imposed.] We compare the exact CFT result, given by the square of Eq. (5.13), with numerical lattice calculations for a free-fermionic chain of length $N = L$ (unit lattice spacing) at half filling for inhomogeneous couplings of the form (5.17). (b) Finite-size scaling of the numerical lattice calculations close to the adiabatic limit, and comparison with the exact CFT result, for $k = 2$, $\lambda = 0.3$, and different system sizes L ranging from 60 to 180 sites. As in Fig. 1, the agreement between numerics and analytical results is striking.

6 Discussion

This work explored the infinite-dimensional quantum geometry of 1+1D gapless many-body quantum systems through the lens of their low-energy dynamics, modeled as driven conformal field theories (CFTs). For slowly driven systems, we showed that the return probability probes the quantum metric through oscillations as a function of the driving frequency: see Figs. 1 and 6. In the complementary limit of arbitrarily fast but weak drives, absorption rates and linear-response coefficients respectively give access to the metric and the Berry curvature of the same quantum geometry. These predictions are universal in the sense that they apply to any 1+1D gapless quantum system with an emergent conformal symmetry at low energies. They hold for both free and strongly interacting systems, and they only depend on the central charge of the effective theory. This is supported by a remarkable agreement between our field-theoretic

results and numerics for gapless lattice models, making the observation of the Virasoro quantum geometry plausible in state-of-the-art quantum simulation experiments.

Some future research directions are worth mentioning:

Geometric formulation of Floquet drives. It was recently understood that Floquet theory can be formulated from a quantum geometric perspective [70], by decomposing the Floquet evolution operator into a purely dynamical part (the ‘average-energy operator’) and a geometric part. It would be interesting to compute the average-energy operator for our periodic drives, and understand the link between the Virasoro Berry phases (4.2) [53] and those of [70].

Higher dimensions. Our study of the quantum geometry of 1+1D gapless many-body quantum systems relied on the Virasoro algebra, allowing us to probe an infinite-dimensional parameter space (2.12). While this algebraic structure is absent in higher-dimensional CFTs, one may still design nonequilibrium probes of the quantum geometry associated with the global conformal group $\text{SO}(d+1, 2)$ of gapless many-body systems in $d+1$ spacetime dimensions. Indeed, given that the approach of this work holds for any continuous symmetry group, it could naturally be applied to higher-dimensional CFTs.

Quantum geometry of mixed states. Our study focused on probes of the quantum geometry of pure states, namely the Virasoro coherent states (2.17). The relevant quantum metric then is the Fubini-Study metric of Sec. 2.3. A natural next step is to consider mixed states instead, and investigate their quantum geometry. In the strict adiabatic regime, one may expect a suitable generalization of our protocol to probe the Uhlmann phase [71, 72], as a mixed state counterpart of the Berry phase. Including subleading corrections in the adiabatic regime should probe the so-called Bogoliubov-Kubo-Mori metric, which was recently studied for thermal initial states in driven CFTs [33].

Acknowledgments

We thank Mathieu Beauvillain, Marin Bukov, Adolfo del Campo, Raphaël Ducatez, Benoit Estienne, Gian Michele Graf, Gregor Jotzu, Bruno Mera, Shinsei Ryu, and Erik Tonni for inspiring discussions. B.L. acknowledges financial support from the Swiss National Science Foundation (Postdoc.Mobility Grant No. 214461). P.M. acknowledges financial support from the Wenner-Gren Foundations (Grant No. FT2022-0002).

A Brief dictionary of CFT formulas

This appendix completes the lightning review of CFT and Virasoro symmetry in Sec. 2. Table 1 summarizes useful CFT formulas in angle coordinates φ, θ vs. length coordinates $x \equiv \frac{L}{2\pi}\varphi$, $y \equiv \frac{L}{2\pi}\theta$. Quantities are distinguished by their arguments, $\delta(\varphi)$ and $\delta(x)$ respectively denote the 2π - and L -periodic delta functions, a prime $'$ denotes differentiation with respect to φ , and $\oint d\phi$ is shorthand for $\int_0^{2\pi} d\phi$. Moreover, $\text{Diff}(S^1)$ denotes the universal cover of the group of orientation-preserving diffeomorphisms of the circle S^1 . $\text{Vect}(S^1)$ denotes the corresponding Lie algebra of real, smooth vector fields on S^1 , and $\text{Vect}(S^1) \otimes \mathbb{C}$ denotes its complexification.

Some context and details for the algebra representation $\mathfrak{u}(\mathbf{X})$ in Table 1 are missing. To fill

	Angle coordinates	Length coordinates
Diff(S^1)	$f(\varphi)$ with $f'(\varphi) > 0$ $f(\varphi + 2\pi) = f(\varphi) + 2\pi$	$f(x) = \frac{L}{2\pi}f(\varphi)$ with $\partial_x f(x) > 0$ $f(x + L) = f(x) + L$
Vect(S^1)	$\mathbf{X} = X(\varphi)\partial_\varphi$, $X(\varphi + 2\pi) = X(\varphi)$ $X(\varphi) = \sum_{n \in \mathbb{Z}} e^{in\varphi} \hat{X}_n$ $\hat{X}_m = \frac{1}{2\pi} \oint d\varphi e^{-im\varphi} X(\varphi)$, $X(\varphi) \in \mathbb{R} \iff \hat{X}_m = \hat{X}_{-m}$ $[\mathbf{X}, \mathbf{Y}] = [X(\varphi)Y'(\varphi) - Y(\varphi)X'(\varphi)]\partial_\varphi$ Infinitesimal $f(\varphi) = \varphi + \epsilon X(\varphi)$	$\mathbf{X} = X(x)\partial_x$, $X(x + L) = X(x)$ $X(x) = \frac{L}{2\pi}X(\varphi) = \frac{L}{2\pi} \sum_{n \in \mathbb{Z}} e^{i\frac{2\pi}{L}nx} \hat{X}_n$ $[\mathbf{X}, \mathbf{Y}] = [X(x)Y'(x) - Y(x)X'(x)]\partial_x$ Infinitesimal $f(x) = x + \epsilon X(x)$
Virasoro algebra	$\mathcal{T}(\varphi) = \frac{1}{2\pi} \sum_{n \in \mathbb{Z}} e^{in\varphi} (L_n - \frac{c}{24}\delta_{n,0})$ $L_m = \oint d\varphi e^{-im\varphi} \mathcal{T}(\varphi) + \frac{c}{24}\delta_{m,0}$ satisfying Eq. (2.9) $[\mathcal{T}(\varphi), \mathcal{T}(\theta)] = -2i\delta'(\varphi - \theta)\mathcal{T}(\theta) + i\delta(\varphi - \theta)\mathcal{T}'(\theta) + \frac{c}{24\pi}i\delta'''(\varphi - \theta)$	$\mathcal{T}(x) = \left(\frac{2\pi}{L}\right)^2 \mathcal{T}(\varphi) = \frac{2\pi}{L^2} \sum_{n \in \mathbb{Z}} e^{i\frac{2\pi}{L}nx} (L_n - \frac{c}{24}\delta_{n,0})$ $[\mathcal{T}(x), \mathcal{T}(y)] = -2i\partial_x \delta(x - y)\mathcal{T}(y) + i\delta(x - y)\partial_y \mathcal{T}(y) + \frac{c}{24\pi}i\partial_x^3 \delta(x - y)$
Proj. rep. $\mathbf{u}(\mathbf{X})$	$\mathbf{u}(\mathbf{X})$ for $\mathbf{X} \in \text{Vect}(S^1)$ or $\text{Vect}(S^1) \otimes \mathbb{C}$ satisfying Eq. (A.2) $i\mathbf{u}(\mathbf{X}) = \int_0^L dx X(x) \mathcal{T}(x) = \sum_{m \in \mathbb{Z}} \hat{X}_m (L_{-m} - \frac{c}{24}\delta_{m,0}) = \oint d\varphi X(\varphi) \mathcal{T}(\varphi)$ $L_n = -\mathbf{u}(\ell_n) + \frac{c}{24}\delta_{n,0}$ for $\ell_n = -ie^{-in\varphi} \partial_\varphi$ satisfying $[\ell_m, \ell_n] = (m - n)\ell_{m+n}$	
Proj. rep. $\mathcal{U}(f)$	$\mathcal{U}(f)$ for $f \in \text{Diff}(S^1)$ satisfying Eq. (2.3) $\mathcal{U}(e^{\lambda \mathbf{X}}) = e^{\lambda \mathbf{u}(\mathbf{X})}$ for $\mathbf{X} \in \text{Vect}(S^1)$, $\lambda \in \mathbb{R}$	

Table 1: CFT formulas in angle coordinates and their counterparts in length coordinates.

this gap, first note that Eq. (2.5) can be written as

$$\mathbf{X} = \sum_{m \in \mathbb{Z}} \hat{X}_m i\ell_{-m} \quad \text{with} \quad \ell_m \equiv -ie^{-im\varphi} \partial_\varphi \quad (\text{A.1})$$

in terms of complexified generators ℓ_m satisfying the commutation relations $[\ell_m, \ell_n] = (m - n)\ell_{m+n}$ of the Witt algebra.¹² Thus, Eq. (2.8) says that $L_m \equiv \mathbf{u}(-\ell_m) + \frac{c}{24}\delta_{m,0}$ represents the (complexified) vector field ℓ_m . Now, owing to the projective composition law (2.3), commutators of the operators (2.6) extend the algebra Vect(S^1) by a central term:

$$[\mathbf{u}(\mathbf{X}), \mathbf{u}(\mathbf{Y})] = \mathbf{u}(-[\mathbf{X}, \mathbf{Y}]) + i\mathbf{c}(\mathbf{X}, \mathbf{Y}) \quad \text{with} \quad \mathbf{c}(\mathbf{X}, \mathbf{Y}) \equiv \oint \frac{d\varphi}{24\pi} X'(\varphi) Y''(\varphi). \quad (\text{A.2})$$

This $\mathbf{c}(\cdot, \cdot)$ is called the Gelfand–Fuchs cocycle; it is the algebra counterpart of the Bott cocycle (2.4). In fact, all nontrivial central extensions of Vect(S^1) by \mathbb{R} are isomorphic and generated by $\mathbf{c}(\cdot, \cdot)$ (see *e.g.* [4]), so the Virasoro central extension is unique up to redefinitions of generators. For the stress-energy tensor $\mathcal{T}(\theta) = i\mathbf{u}(\delta(\varphi - \theta)\partial_\varphi)$, Eq. (A.2) yields

$$[\mathcal{T}(\varphi), \mathcal{T}(\theta)] = -2i\delta'(\varphi - \theta)\mathcal{T}(\theta) + i\delta(\varphi - \theta)\mathcal{T}'(\theta) + \frac{c}{24\pi}i\delta'''(\varphi - \theta), \quad (\text{A.3})$$

which are nothing but the Virasoro commutation relations (2.9) upon using Eq. (2.7). Lastly, we note that the Hermiticity $L_m^\dagger = L_{-m}$ follows directly from the unitarity of $\mathcal{U}(\cdot)$, or equivalently from the anti-Hermiticity of $\mathbf{u}(\cdot)$.

¹²This is the subalgebra $\text{span}_{\mathbb{C}}(\{\ell_n\}_{n \in \mathbb{Z}})$ of the complexification Vect(S^1) $\otimes \mathbb{C}$. Note the isomorphism of the Witt algebra under $\ell_n \mapsto -\ell_{-n}$. This does not carry over to the Virasoro algebra (2.9) since its central term changes sign.

B Virasoro quantum geometry away from the identity

In this appendix, we briefly describe the quantum metric and the Berry curvature of a homogeneous parameter space (2.20) at points away from the identity. We then apply this to the case (2.12) that is relevant for Virasoro quantum geometry.

General case. Let G be a Lie group, \mathcal{U} a unitary representation of G , and consider the parameter space (2.20) for ‘deformed’ Hamiltonians of the form $\mathcal{U}(f)H_0\mathcal{U}(f)^{-1}$. We saw in Sec. 2 that the ensuing quantum metric and Berry curvature at the identity are given by Eq. (2.21). When evaluated at the coset fG_0 in the space (2.20), the metric and the curvature are given by

$$\mathcal{G} = -\langle h|\mathfrak{u}(f^{-1}df) \odot \mathfrak{u}(f^{-1}df)|h\rangle + \langle h|\mathfrak{u}(f^{-1}df)|h\rangle \odot \langle h|\mathfrak{u}(f^{-1}df)|h\rangle, \quad (\text{B.1a})$$

$$\mathcal{F} = 2i\langle h|\mathfrak{u}(f^{-1}df) \wedge \mathfrak{u}(f^{-1}df)|h\rangle, \quad (\text{B.1b})$$

where $\mathfrak{u}(f^{-1}df)$ is the representation of the left Maurer-Cartan form $f^{-1}df$ on G . The latter is the map $f^{-1}df : T_f G \rightarrow \mathfrak{g}$ such that, for any path $\gamma(t)$ in G for which $\gamma(0) = f$, one has

$$f^{-1}df(\partial_t \gamma|_{t=0}) \equiv \partial_t(f^{-1} \cdot \gamma(t))|_{t=0} \quad (\text{B.2})$$

with the dot \cdot denoting multiplication in G .

Virasoro case. For $G = \text{Diff}(S^1)$, the metric and the curvature at the identity are given by Eqs. (2.22)–(2.25). Let us now extend these expressions to the whole parameter space (2.12). Owing to Eq. (B.1), this is essentially achieved by replacing \mathbf{X}, \mathbf{Y} in Eqs. (2.24)–(2.25) by the left Maurer-Cartan form $f^{-1}df$, and including tensor products where and when they are needed. Let us first discuss the Maurer-Cartan form in its own right. As briefly explained below Eq. (B.1), $f^{-1}df$ is a Lie-algebra-valued one-form; so, for $G = \text{Diff}(S^1)$, it takes values in the space $\mathfrak{g} = \text{Vect}(S^1)$ of vector fields on the circle. Any tangent vector at $f \in \text{Diff}(S^1)$ can be seen as the time derivative $\partial_t \gamma_t|_{t=0}$ of a path γ_t in $\text{Diff}(S^1)$ such that $\gamma_0 = f$. This allows us to write the left Maurer-Cartan form on $\text{Diff}(S^1)$ by adapting Eq. (B.2) to a group operation given by the composition of functions:

$$f^{-1}df(\partial_t \gamma_t|_{t=0}) \equiv \partial_t(f^{-1} \circ \gamma_t)|_{t=0} = \frac{\partial_t \gamma_t(\varphi)|_{t=0}}{f'(\varphi)} \partial_\varphi. \quad (\text{B.3})$$

Here we used the chain rule to obtain the last equality. As expected, the Maurer-Cartan form is vector-field-valued. Henceforth, we write it as

$$f^{-1}df \equiv \frac{\delta f(\varphi)}{f'(\varphi)} \partial_\varphi, \quad (\text{B.4})$$

with the functional differential δf emphasizing that the one-form acts on a space of functions.

The compact notation (B.4) can now be combined with Eqs. (2.24)–(2.25) to express the quantum metric and the Berry curvature at any point f in the group manifold $\text{Diff}(S^1)$ [or more precisely at any coset $f \circ S^1$ in the parameter space (2.12)]. Namely,

$$\mathcal{G} = \oint \frac{d\varphi d\theta}{16\pi^2} \frac{(h - \frac{c}{24}) \left(\left. \frac{\delta f}{f'} \right|_\varphi - \left. \frac{\delta f}{f'} \right|_\theta \right)^2 + \frac{c}{24} \left(\left(\left. \frac{\delta f}{f'} \right|_\varphi - \left. \frac{\delta f}{f'} \right|_\theta \right)' \right)^2}{\sin^2[(\theta - \varphi)/2]}, \quad (\text{B.5a})$$

$$\mathcal{F} = -2 \oint \frac{d\varphi}{2\pi} \left[\left(h - \frac{c}{24} \right) \frac{\delta f}{f'} \wedge \left(\frac{\delta f}{f'} \right)' - \frac{c}{24} \frac{\delta f}{f'} \wedge \left(\frac{\delta f}{f'} \right)''' \right], \quad (\text{B.5b})$$

where we use the notation $\delta f^2 \equiv \delta f \odot \delta f$ for symmetrized products of one-forms. These expressions are explicit in principle, but complicated to use in practice. Again, the main lesson is that both of these tensor fields are fully determined by their value at the identity. In particular, we saw in Sec. 4 that the return probability of a slowly driven quantum state involves the quantum metric evaluated at a point f far away from the identity, even though the actual formula involves the much simpler metric in Eqs. (2.22a) or (2.25) at the identity.

C Linear response to Virasoro drives

The goal here is to derive the linear-response result (3.8) and its gradient expansion (3.11). The first step is to write the Hamiltonian in Eq. (3.2) as $H(t) = H_0 + V_S(t) + O(\epsilon^2)$ with

$$V_S(t) \equiv \epsilon [\mathfrak{u}(\mathbf{X}_t), H_0] = \epsilon \frac{2\pi}{L} [\mathfrak{u}(\mathbf{X}_t), L_0] = i\epsilon \frac{2\pi}{L} \sum_{n \neq 0} n \hat{X}_n(t) L_{-n}, \quad (\text{C.1})$$

where \mathbf{X}_t is an arbitrary time-dependent vector field. As in the main text, let $|\phi(0)\rangle = |h\rangle$ be the initial state and consider the solution $|\phi(t)\rangle$ of the Schrödinger equation at time t , under the full $H(t)$ dynamics.

Susceptibility. Since we wish to compute $\langle \phi(t) | i\mathfrak{u}(\mathbf{Y}) | \phi(t) \rangle$ for any vector field \mathbf{Y} , it suffices to study the single-mode expectation value

$$\langle \phi(t) | L_{-m} | \phi(t) \rangle \quad (\text{C.2})$$

for any given integer m . [Indeed, $i\mathfrak{u}(\mathbf{Y})$ is a linear combination of L_m s in Eq. (2.8).] To this end, we work in the interaction picture and define

$$V_I(t) \equiv e^{iH_0 t} V_S(t) e^{-iH_0 t} = i\epsilon \frac{2\pi}{L} \sum_{n \neq 0} n \hat{X}_n(t) L_{-n}^I(t) = i\epsilon \frac{2\pi}{L} \sum_{n \neq 0} n \hat{X}_n(t) L_{-n} e^{i2\pi nt/L}, \quad (\text{C.3})$$

with $L_m^I(t) \equiv e^{iH_0 t} L_m e^{-iH_0 t} = L_m e^{-i2\pi mt/L}$ obtained by solving $\partial_t L_m^I(t) = -i\frac{2\pi}{L} m L_m^I(t)$ with $L_m^I(0) = L_m$. Thus,

$$\langle \phi(t) | L_{-m} | \phi(t) \rangle = \langle h | U_I(t)^{-1} L_{-m}^I(t) U_I(t) | h \rangle \quad (\text{C.4})$$

where the evolution operator $U_I(t)$ is expressible using the Dyson formula

$$U_I(t) = I - i \int_0^t ds V_I(s) + O(\epsilon^2). \quad (\text{C.5})$$

This gives the Dyson series

$$\begin{aligned} \langle \phi(t) | L_{-m} | \phi(t) \rangle &= \langle h | L_{-m}^I(t) | h \rangle + i \int_0^t ds \langle h | [V_I(s), L_{-m}^I(t)] | h \rangle + O(\epsilon^2) \\ &= \langle h | L_{-m} | h \rangle e^{i2\pi mt/L} + i\epsilon \frac{2\pi}{L} \sum_{n \neq 0} \int_0^t ds n \hat{X}_n(s) \mathcal{F}_{m,n} e^{i2\pi(mt+ns)/L} + O(\epsilon^2) \\ &= \langle h | L_{-m} | h \rangle e^{i2\pi mt/L} + \epsilon \sum_{n \neq 0} \int_0^t ds \chi_{m,n}(t, s) \hat{X}_n(s) + O(\epsilon^2), \end{aligned} \quad (\text{C.6})$$

where we identified the Berry curvature $\mathcal{F}_{m,n}$ of Eq. (2.23b) and the susceptibility $\chi_{m,n}(t, s)$ of Eq. (3.9). The result (3.8) for operators $i\mathfrak{u}(\mathbf{Y})$ with Fourier components $\hat{Y}_m = \hat{Y}_{-m}^*$ follows.

Gradient expansion. It remains to derive the gradient expansion (3.11). To this end, we use repeated integration by parts starting from Eq. (C.6), which yields

$$\begin{aligned} \langle \phi(t) | L_{-m} | \phi(t) \rangle &= \langle h | L_{-m} | h \rangle e^{i2\pi m t / L} + \epsilon \sum_{n \neq 0} \mathcal{F}_{m,n} \left[\hat{X}_n(s) e^{i2\pi(m t + n s) / L} \right]_{s=0}^t \\ &\quad + \epsilon \sum_{n \neq 0} \mathcal{F}_{m,n} \sum_{k=1}^N \left(-\frac{L}{2\pi i n} \right)^k \left[[\partial_s^k \hat{X}_n(s)] e^{i2\pi(m t + n s) / L} \right]_{s=0}^t + R_m^{(N)}(t) + O(\epsilon^2) \end{aligned} \quad (\text{C.7})$$

for $N \geq 1$, with the remainder term

$$R_m^{(N)}(t) = -\epsilon \sum_{n \neq 0} \mathcal{F}_{m,n} \left(-\frac{L}{2\pi i n} \right)^N \int_0^t ds [\partial_s^{N+1} \hat{X}_n(s)] e^{i2\pi(m t + n s) / L}. \quad (\text{C.8})$$

Since $\mathcal{F}_{m,n}$ is zero if $m = 0$ (or $n = 0$), it follows from the above that

$$\begin{aligned} \langle \phi(t) | i\mathbf{u}(\mathbf{Y}) | \phi(t) \rangle &= \langle h | i\mathbf{u}(\mathbf{Y}) | h \rangle e^{i2\pi m t / L} + \epsilon \sum_{m,n \neq 0} \hat{Y}_m \mathcal{F}_{m,n} \left[\hat{X}_n(s) e^{i2\pi(m t + n s) / L} \right]_{s=0}^t \\ &\quad + \epsilon \sum_{m,n \neq 0} \hat{Y}_m \mathcal{F}_{m,n} \sum_{k=1}^N \left(-\frac{L}{2\pi i n} \right)^k \left[[\partial_s^k \hat{X}_n(s)] e^{i2\pi(m t + n s) / L} \right]_{s=0}^t + \sum_{m \neq 0} \hat{Y}_m R_m^{(N)}(t) + O(\epsilon^2). \end{aligned} \quad (\text{C.9})$$

This implies Eq. (3.11) since $\mathcal{F}_{m,n}$ is zero unless $m + n = 0$.

D Rotating $\text{SL}(2, \mathbb{R})$ drives

This appendix completes Sec. 5, for which it provides the explicit matrix expressions mentioned there.

Hamiltonian as a matrix. Our starting point is the Hamiltonian (5.3) expressed as

$$H(t) = \frac{2\pi k}{L} \left[\cosh(2\lambda) K_0 + \frac{i}{2} \sinh(2\lambda) \left(e^{ik\omega t} K_- - e^{-ik\omega t} K_+ \right) \right] - \frac{\pi c}{12L} k^2 \quad (\text{D.1})$$

in terms of the following generators of $\mathfrak{su}(1, 1) \cong \mathfrak{sl}(2, \mathbb{R})$ [46, 73, 74]:

$$K_0 \equiv \frac{1}{k} \left[L_0 + \frac{c}{24} (k^2 - 1) \right], \quad K_- \equiv \frac{i}{k} L_k, \quad K_+ \equiv -\frac{i}{k} L_{-k}. \quad (\text{D.2})$$

These satisfy the usual $\mathfrak{su}(1, 1)$ relations

$$[K_-, K_+] = 2K_0, \quad [K_0, K_{\pm}] = \pm K_{\pm}, \quad K_0^\dagger = K_0, \quad K_-^\dagger = K_+. \quad (\text{D.3})$$

By convention, the generators K_{\pm} have a factor i , meaning that the corresponding coefficients $\beta_{\pm} = \mp \frac{i\pi k}{L} \sinh(2\lambda) e^{\mp ik\omega t}$ in Eq. (D.1) satisfy $\overline{\beta_+} = \beta_-$.

To make analytical progress, we use the fundamental, nonunitary representation of $\mathfrak{su}(1, 1)$ in terms of 2×2 -matrices:

$$K_0 \big|_{2 \times 2} = \begin{pmatrix} -1/2 & 0 \\ 0 & 1/2 \end{pmatrix}, \quad K_- \big|_{2 \times 2} = \begin{pmatrix} 0 & 1 \\ 0 & 0 \end{pmatrix}, \quad K_+ \big|_{2 \times 2} = \begin{pmatrix} 0 & 0 \\ -1 & 0 \end{pmatrix}. \quad (\text{D.4})$$

The Hamiltonian (D.1) in this picture reads

$$H(t)|_{2 \times 2} = \frac{\pi k}{L} \begin{pmatrix} -\cosh(2\lambda) - ck/12 & i \sinh(2\lambda) e^{ik\omega t} \\ i \sinh(2\lambda) e^{-ik\omega t} & \cosh(2\lambda) - ck/12 \end{pmatrix}. \quad (\text{D.5})$$

Naturally, this finite-dimensional representation is nonunitary since $\mathfrak{sl}(1, 1)$ is noncompact—manifested already in Eq. (D.5) as the matrix is not Hermitian. However, as Eq. (D.4) is the fundamental representation of $\mathfrak{su}(1, 1)$, it is faithful, so any lesson learned for this representation holds in general for $\mathfrak{su}(1, 1)$.

Evolution operator. By definition of time-ordered exponentials as product integrals, the time-evolution operator (5.4) can be represented as in Eq. (5.5):

$$U(t)|_{2 \times 2} = e^{i \frac{\pi c}{12L} k^2 t} \lim_{M \rightarrow \infty} \overleftarrow{\prod}_{m=0, \dots, M} \exp \left[\frac{\pi k}{L} \delta t \begin{pmatrix} i \cosh(2\lambda) & \sinh(2\lambda) e^{ik\omega m \delta t} \\ \sinh(2\lambda) e^{-ik\omega m \delta t} & -i \cosh(2\lambda) \end{pmatrix} \right], \quad (\text{D.6})$$

where $\delta t \equiv t/M$ and the product $\overleftarrow{\prod}$ is ordered so that time decreases from left to right. Noting that any dependence on m is contained in the phases $e^{\pm ik\omega m \delta t}$, we use

$$\begin{pmatrix} 0 & e^{-i\omega s/2} \\ e^{i\omega s/2} & 0 \end{pmatrix} \begin{pmatrix} -i\bar{\alpha} & \bar{\beta} \\ \beta & i\alpha \end{pmatrix} \begin{pmatrix} 0 & e^{-i\omega s/2} \\ e^{i\omega s/2} & 0 \end{pmatrix} = \begin{pmatrix} i\alpha & \beta e^{-i\omega s} \\ \bar{\beta} e^{i\omega t} & -i\bar{\alpha} \end{pmatrix} \quad (\text{D.7})$$

for $s = -km\delta t$ and $\alpha = \cosh(2\lambda)$, $\beta = \sinh(2\lambda)$ to rewrite each factor in Eq. (D.6). As a result, each pair of consecutive factors gives rise to products of the form

$$\begin{pmatrix} 0 & e^{ik\omega(m+1)\delta t/2} \\ e^{-ik\omega(m+1)\delta t/2} & 0 \end{pmatrix} \begin{pmatrix} 0 & e^{ik\omega m \delta t/2} \\ e^{-ik\omega m \delta t/2} & 0 \end{pmatrix} = \begin{pmatrix} e^{ik\omega \delta t/2} & 0 \\ 0 & e^{ik\omega \delta t/2} \end{pmatrix}, \quad (\text{D.8})$$

which thus are independent of m . The latter observation is crucial, since it implies that

$$U(t)|_{2 \times 2} = e^{i \frac{\pi c}{12L} k^2 t} \lim_{M \rightarrow \infty} \begin{pmatrix} 0 & e^{ik\omega t/2} \\ e^{-ik\omega t/2} & 0 \end{pmatrix} \mathsf{A}^M \exp \left[\frac{\pi k}{L} \delta t \begin{pmatrix} -i \cosh(2\lambda) & \sinh(2\lambda) \\ \sinh(2\lambda) & i \cosh(2\lambda) \end{pmatrix} \right] \begin{pmatrix} 0 & 1 \\ 1 & 0 \end{pmatrix}, \quad (\text{D.9})$$

where

$$\mathsf{A} = \exp \left[\frac{\pi k}{L} \delta t \begin{pmatrix} -i \cosh(2\lambda) & \sinh(2\lambda) \\ \sinh(2\lambda) & i \cosh(2\lambda) \end{pmatrix} \right] \begin{pmatrix} e^{ik\omega \delta t/2} & 0 \\ 0 & -e^{ik\omega \delta t/2} \end{pmatrix} = \begin{pmatrix} a & b \\ \bar{b} & \bar{a} \end{pmatrix} + O(\delta t^2) \quad (\text{D.10})$$

with $a = [1 - i(\pi k/L)\delta t \cosh(2\lambda)] e^{ik\omega \delta t/2}$ and $b = (\pi k/L)\delta t \sinh(2\lambda) e^{-ik\omega \delta t/2}$. Diagonalizing A , noting that all $O(\delta t^2)$ contributions give rise to subleading corrections in $1/M$, yields

$$U(t)|_{2 \times 2} = e^{i \frac{\pi c}{12L} k^2 t} \begin{pmatrix} e^{ik\omega t/2} & 0 \\ 0 & e^{-ik\omega t/2} \end{pmatrix} \times \begin{pmatrix} \cos(k\Omega t/2) + i \frac{\cosh(2\lambda) - L/T}{L\Omega/2\pi} \sin(k\Omega t/2) & \frac{\sinh(2\lambda)}{L\Omega/2\pi} \sin(k\Omega t/2) \\ \frac{\sinh(2\lambda)}{L\Omega/2\pi} \sin(k\Omega t/2) & \cos(k\Omega t/2) - i \frac{\cosh(2\lambda) - L/T}{L\Omega/2\pi} \sin(k\Omega t/2) \end{pmatrix}, \quad (\text{D.11})$$

where we used $\lim_{M \rightarrow \infty} (1 + \kappa/M)^{\mu M} = e^{\mu\kappa}$ for $\kappa, \mu \in \mathbb{R}$.

Now exploiting the fundamental representation (D.4) and the ansatz $e^{i[G + \bar{F}L_{-k} + EL_0 + FL_k]}|_{2 \times 2}$ ($G, E \in \mathbb{R}, F \in \mathbb{C}$) for the second matrix in Eq. (D.11), one can show that Eq. (5.6) holds for the evolution operator. This can also be used to find the diffeomorphism $g_t \in \text{Diff}(S^1)$ corresponding to the two last exponentials in Eq. (5.6). Owing to the properties of one-parameter flows, one can indeed show that $U(t) = e^{i\alpha t} \mathcal{U}(g_t) \mathcal{U}(g_0)^{-1}$ with g_t of the form (4.14), where $\zeta(\varphi)$ is a transformation (5.1) with α, β as in Eq. (5.7) and Ω is given by Eq. (5.8).

Return amplitudes. When the initial condition is $g_0 = f_0$, we also need to express $\mathcal{U}(f_0)$ appearing in the initial state $|\psi(0)\rangle = \mathcal{U}(f_0)|h\rangle$ for f_0 of the $\text{SL}(2, \mathbb{R})$ form (5.1) with $\alpha = \cosh(\lambda)$, $\beta = \sinh(\lambda)$ as a 2×2 matrix. Since f_0 is the one-parameter flow generated by $-(2/k)\sin(k\varphi)\partial_\varphi$ with respect to λ , one finds

$$\mathcal{U}(f_0)|_{2 \times 2} = \exp\left(\frac{\lambda}{k}[L_{-k} - L_k]\right)|_{2 \times 2} = \begin{pmatrix} \cosh(\lambda) & i \sinh(\lambda) \\ -i \sinh(\lambda) & \cosh(\lambda) \end{pmatrix}. \quad (\text{D.12})$$

Replicating the steps that led to Eq. (5.6), the above can be used to factorize

$$U(t)\mathcal{U}(f_0) = e^{i\rho_t} e^{\chi_t L_{-k} - \bar{\chi}_t L_k} e^{i\sigma_t L_0}, \quad (\text{D.13})$$

where

$$\rho_t = \frac{\pi c}{12L} \left[k^2 t + \frac{L\sigma_t}{2\pi} (k^2 - 1) \right], \quad \sigma_t = -\omega t - \frac{2}{k} \arctan\left(\left[\frac{2\pi}{L\Omega} - \frac{\omega}{\Omega}\right] \tan(k\Omega t/2)\right), \quad (\text{D.14})$$

and η_t in (5.10), with Ω given in Eq. (5.8). Evaluating $U(t)\mathcal{U}(f_0)|h\rangle$ yields Eq. (5.9), after factoring out an overall phase that is equal to $\rho_t + h\sigma_t$ due to Eq. (2.16).

Lastly, combining Eqs. (D.11) and (D.12) allows us to represent $\mathcal{U}(f_0)^{-1}U(t)\mathcal{U}(f_0)$ as an $\text{SU}(1, 1)$ matrix:

$$\mathcal{U}(f_0)^{-1}U(t)\mathcal{U}(f_0)|_{2 \times 2} = \begin{pmatrix} u_t & w_t \\ \bar{w}_t & \bar{u}_t \end{pmatrix} \quad (\text{D.15})$$

with u_t as in Eq. (5.14) and $w_t = \sinh(2\lambda) \left[\frac{\omega}{\Omega} \sin(k\Omega t/2) \cos(k\omega t/2) - \cos(k\Omega t/2) \sin(k\omega t/2) + i \frac{2\pi}{L\Omega} \sin(k\Omega t/2) \sin(k\omega t/2) \right]$. On general grounds, this must be the nonunitary 2×2 -matrix representation of an element of the form $e^D e^{AL_{-k}} e^{BL_0} e^{CL_k}$, which implies

$$A = \frac{i}{k} \frac{\bar{w}}{u}, \quad B = -\frac{2}{k} \log(u), \quad C = \frac{i}{k} \frac{w}{u}, \quad e^D = e^{i \frac{\pi c}{12L} k^2 t} e^{B \frac{c}{24} (k^2 - 1)}. \quad (\text{D.16})$$

It follows using Eq. (2.16) that

$$\langle \psi(0)|\psi(t)\rangle = \langle h|\mathcal{U}(f_0)^{-1}U(t)\mathcal{U}(f_0)|h\rangle = e^D \langle h|e^{BL_0}|h\rangle = e^{D+Bh}, \quad (\text{D.17})$$

which yields Eq. (5.13).

E Lattice calculations

Let us finally provide details on the numerics used throughout this work.

Lattice Hamiltonian. We consider a driven inhomogeneous free-fermion chain at half-filling. Given fermionic creation (annihilation) operators c_j^\dagger (c_j) acting on sites $j = 1, \dots, N$ and satisfying the usual anticommutation relations $\{c_j, c_{j'}^\dagger\} = \delta_{j,j'}$ and $\{c_j, c_{j'}\} = \{c_j^\dagger, c_{j'}^\dagger\} = 0$, the Hamiltonian is

$$H_N(t) = -\frac{1}{2} \sum_{j=1}^N J_j(t) \left(c_j^\dagger c_{j+1} + \text{h.c.} \right) \quad (\text{E.1})$$

with inhomogeneous nearest-neighbor couplings $J_j(t) = J_j(t+T) > 0$ and periodic boundary conditions, $c_{N+1}^\dagger = c_1^\dagger$ and $J_{N+1}(t) = J_1(t)$. This model can be mapped (up to boundary terms) to the inhomogeneous spin chain in Eq. (1.2) with $\Delta = 0$ via a Jordan-Wigner transformation. Assuming that the system size L is much larger than the lattice spacing L/N , *i.e.* $N \gg 1$, and that $J_j(t)$ vary on mesoscopic length scales, the model (E.1) can be effectively described in the low-energy regime by an inhomogeneous CFT (1.1) with $c = 1$ but involving both the right- and left-moving (chiral and antichiral) components of the CFT [26].

Return probabilities. In our lattice calculations, we only consider the fermions at zero temperature, meaning that our CFT results should be a good approximation of the lattice dynamics. Concretely, we let $|\psi_N(0)\rangle$ be the ground state of $H_N(0)$, which in the CFT language corresponds to a coherent state in the vacuum superselection sector ($h = \bar{h} = 0$), and calculate the return probability

$$\left| \langle \psi_N(0) | \psi_N(T) \rangle \right|^2 = \left| \langle \psi_N(0) | U_N(T) | \psi_N(0) \rangle \right|^2, \quad U_N(T) \equiv \overleftarrow{\mathcal{T}} e^{-i \int_0^T dt H_N(t)} \quad (\text{E.2})$$

after one period T . To this end, as is commonplace, we exploit the fact that the Hamiltonian for any periodic fermionic chain with nearest-neighbor couplings can be represented by a periodic Jacobi matrix. In our case, since there is no external field, this appears as the adjacency matrix

$$\mathbf{J}(t) \equiv \begin{pmatrix} 0 & J_1(t) & 0 & \dots & 0 & J_N(t) \\ J_1(t) & 0 & J_2(t) & \dots & 0 & 0 \\ 0 & J_2(t) & 0 & \dots & 0 & 0 \\ \vdots & \vdots & \vdots & \ddots & \vdots & \vdots \\ 0 & 0 & 0 & \dots & 0 & J_{N-1}(t) \\ J_N(t) & 0 & 0 & \dots & J_{N-1}(t) & 0 \end{pmatrix}, \quad (\text{E.3})$$

which allows us to write $H_N(t) = (c_1^\dagger, c_2^\dagger, \dots, c_N^\dagger) \mathbf{H}(t) (c_1, c_2, \dots, c_N)^T$ with $\mathbf{H}(t) \equiv -\mathbf{J}(t)/2$ interpreted as a single-particle Hamiltonian. Let \mathbf{U} be the unitary matrix that diagonalizes $\mathbf{H}(t)$ at time $t = 0$. It follows that

$$H_N(0) = \sum_{j=1}^N E_j(0) \gamma_j^\dagger \gamma_j, \quad \gamma_j = \sum_{\ell=1}^N (\mathbf{U}^\dagger)_{j\ell} c_\ell \quad (\text{E.4})$$

with eigenenergies $E_j(0)$ of $\mathbf{H}(0)$ and new fermionic creation (annihilation) operators γ_j^\dagger (γ_j). General properties for periodic Jacobi matrices [75] imply that the $E_j(0)$ can be ordered to be (nonstrictly) increasing in $j = 1, \dots, N$ (with each eigenenergy equal to at most one other).

Recall that half filling corresponds to filling all single-particle states with negative energies. For simplicity, let N be even. Then, all states with $j = 1, \dots, N/2$ have nonpositive energies,¹³ *i.e.* the ground state at half-filling can be taken as $|\psi_N(0)\rangle = \prod_{j=1}^{N/2} \gamma_j^\dagger |\text{vac}\rangle$, where $|\text{vac}\rangle$ denotes the state with no fermions. (For N odd, one must replace $N/2$ by the maximal value N_{max} so that $E_{N_{\text{max}}}(0)$ is negative.) It follows that the return probability (E.2) reduces to computing

$$\begin{aligned} & \left| \langle \text{vac} | \gamma_1 \dots \gamma_{N/2} U_N(T) \gamma_{N/2}^\dagger \dots \gamma_1^\dagger | \text{vac} \rangle \right|^2 \\ &= \left| \langle \text{vac} | [U_N(T)^\dagger \gamma_1 U_N(T)] \dots [U_N(T)^\dagger \gamma_{N/2} U_N(T)] \gamma_{N/2}^\dagger \dots \gamma_1^\dagger | \text{vac} \rangle \right|^2. \quad (\text{E.5}) \end{aligned}$$

To find $U_N(T)^\dagger \gamma_j U_N(T)$, we need to discretize the continuous time evolution: we approximate the evolution under $H_N(t)$ for one period as one consisting of $M \gg 1$ time steps, each evolved under a static Hamiltonian $H_N(m\delta t)$ for a time $\delta t = T/M$. In other words,

$$U_N(T) \approx \prod_{m=0}^M e^{-i H_N(m\delta t) \delta t}. \quad (\text{E.6})$$

¹³For N even, let $S = \text{diag}(1, -1, 1, -1, \dots, 1, -1)$. Since $\mathbf{J}(t)$ in Eq. (E.3) satisfies $\mathbf{S}\mathbf{J}(t) = -\mathbf{J}(t)\mathbf{S}$, if \mathbf{x} is an eigenvector of $\mathbf{H}(t) = -\mathbf{J}(t)/2$ with eigenvalue E , then $\mathbf{S}\mathbf{x}$ is also an eigenvector with eigenvalue $-E$.

As when $t = 0$, the single-particle Hamiltonian $\mathsf{H}(m\delta t)$ corresponding to $H_N(m\delta t)$ can be diagonalized by a unitary matrix V_m . Let $E_j(m\delta t)$ denote the eigenenergies of $\mathsf{H}(m\delta t)$. Defining $\mathsf{W}_m(\delta t) \equiv \mathsf{U}^\dagger \mathsf{V}_m \text{diag}(e^{-iE_1(m\delta t)\delta t}, \dots, e^{-iE_N(m\delta t)\delta t}) \mathsf{V}_m^\dagger \mathsf{U}$, it follows that

$$e^{iH_N(m\delta t)\delta t} \gamma_j e^{-iH_N(m\delta t)\delta t} = \sum_{\ell=1}^N \left(\mathsf{W}_m(\delta t) \right)_{j\ell} \gamma_\ell. \quad (\text{E.7})$$

We use this decomposition for each time step in Eq. (E.5), which reduces the whole calculation to evaluating a correlator for the γ_ℓ s. The return probability can then be approximated as

$$\left| \langle \psi_N(0) | \psi_N(T) \rangle \right|^2 \approx \left| \det_{1 \leq i, \ell \leq N/2} \left(\prod_{m=0}^M \mathsf{W}_m(\delta t) \right)_{j\ell} \right|^2 \quad (\text{E.8})$$

with the help of Wick's theorem.

References

- [1] V. Arnold. Sur la géométrie différentielle des groupes de Lie de dimension infinie et ses applications à l'hydrodynamique des fluides parfaits. *Ann. Inst. Fourier* **16**, 319 (1966).
- [2] V. I. Arnold. [On the differential geometry of infinite-dimensional Lie groups and its application to the hydrodynamics of perfect fluids](#). In *Vladimir I. Arnold - Collected Works, Vol. 2*, p. 33. Springer, Berlin, Heidelberg (1966).
- [3] M. Adams, T. Ratiu, and R. Schmid. [The Lie group structure of diffeomorphism groups and invertible Fourier integral operators with applications](#). In *Infinite Dimensional Groups with Applications*, Mathematical Sciences Research Institute Publications, Vol. 4, p. 1. Springer, New York (1985).
- [4] B. Khesin and R. Wendt. *The Geometry of Infinite-Dimensional Groups*. Springer, Berlin, Heidelberg (2009).
- [5] B. Khesin, G. Misiołek, and K. Modin. Geometric hydrodynamics and infinite-dimensional Newton,Åôs equations. *Bull. Amer. Math. Soc.* **58**, 377 (2021).
- [6] J. P. Provost and G. Vallee. Riemannian structure on manifolds of quantum states. *Commun. Math. Phys.* **76**, 289 (1980).
- [7] J. Anandan and Y. Aharonov. Geometry of quantum evolution. *Phys. Rev. Lett.* **65**, 1697 (1990).
- [8] N. Marzari and D. Vanderbilt. Maximally localized generalized Wannier functions for composite energy bands. *Phys. Rev. B* **56**, 12847 (1997).
- [9] R. Resta and S. Sorella. Electron localization in the insulating state. *Phys. Rev. Lett.* **82**, 370 (1999).
- [10] I. Souza, T. Wilkens, and R. M. Martin. Polarization and localization in insulators: Generating function approach. *Phys. Rev. B* **62**, 1666 (2000).
- [11] F. D. M. Haldane. Geometrical description of the fractional quantum Hall effect. *Phys. Rev. Lett.* **107**, 116801 (2011).
- [12] R. Roy. Band geometry of fractional topological insulators. *Phys. Rev. B* **90**, 165139 (2014).

- [13] S. Peotta and P. Törmä. Superfluidity in topologically nontrivial flat bands. *Nat. Commun.* **6**, 8944 (2015).
- [14] F. Xie, Z. Song, B. Lian, and B. A. Bernevig. Topology-bounded superfluid weight in twisted bilayer graphene. *Phys. Rev. Lett.* **124**, 167002 (2020).
- [15] T. Ozawa and B. Mera. Relations between topology and the quantum metric for Chern insulators. *Phys. Rev. B* **104**, 045103 (2021).
- [16] B. Mera and T. Ozawa. Kähler geometry and Chern insulators: Relations between topology and the quantum metric. *Phys. Rev. B* **104**, 045104 (2021).
- [17] J. Yu, B. A. Bernevig, R. Queiroz, E. Rossi, P. Törmä, and B.-J. Yang. Quantum geometry in quantum materials. *npj Quantum Mater.* **10**, 101 (2025).
- [18] T. Giamarchi. *Quantum Physics in One Dimension*. Oxford University Press, Oxford (2003).
- [19] M. A. Cazalilla, R. Citro, T. Giamarchi, E. Orignac, and M. Rigol. One dimensional bosons: From condensed matter systems to ultracold gases. *Rev. Mod. Phys.* **83**, 1405 (2011).
- [20] A. A. Belavin, A. M. Polyakov, and A. B. Zamolodchikov. Infinite conformal symmetry in two-dimensional quantum field theory. *Nucl. Phys. B* **241**, 333 (1984).
- [21] N. Allegra, J. Dubail, J.-M. Stéphan, and J. Viti. Inhomogeneous field theory inside the arctic circle. *J. Stat. Mech.* **2016**, 053108 (2016).
- [22] J. Dubail, J.-M. Stéphan, J. Viti, and P. Calabrese. Conformal field theory for inhomogeneous one-dimensional quantum systems: The example of non-interacting Fermi gases. *SciPost Phys.* **2**, 002 (2017).
- [23] J. Dubail, J.-M. Stéphan, and P. Calabrese. Emergence of curved light-cones in a class of inhomogeneous Luttinger liquids. *SciPost Phys.* **3**, 019 (2017).
- [24] K. Gawędzki, E. Langmann, and P. Moosavi. Finite-time universality in nonequilibrium CFT. *J. Stat. Phys.* **172**, 353 (2018).
- [25] E. Langmann and P. Moosavi. Diffusive heat waves in random conformal field theory. *Phys. Rev. Lett.* **122**, 020201 (2019).
- [26] P. Moosavi. Inhomogeneous conformal field theory out of equilibrium. *Ann. Henri Poincaré* **25**, 1083 (2024).
- [27] X. Wen and J.-Q. Wu. *Floquet conformal field theory*. arXiv:1805.00031 [cond-mat.str-el] (2018).
- [28] R. Fan, Y. Gu, A. Vishwanath, and X. Wen. Emergent spatial structure and entanglement localization in Floquet conformal field theory. *Phys. Rev. X* **10**, 031036 (2020).
- [29] B. Lapierre, K. Choo, C. Tauber, A. Tiwari, T. Neupert, and R. Chitra. Emergent black hole dynamics in critical Floquet systems. *Phys. Rev. Res.* **2**, 023085 (2020).
- [30] B. Lapierre and P. Moosavi. Geometric approach to inhomogeneous Floquet systems. *Phys. Rev. B* **103**, 224303 (2021).
- [31] X. Wen, R. Fan, A. Vishwanath, and Y. Gu. Periodically, quasiperiodically, and randomly driven conformal field theories. *Phys. Rev. Res.* **3**, 023044 (2021).
- [32] R. Fan, Y. Gu, A. Vishwanath, and X. Wen. Floquet conformal field theories with generally deformed Hamiltonians. *SciPost Phys.* **10**, 049 (2021).
- [33] J. de Boer, V. Godet, J. Kastikainen, and E. Keski-Vakkuri. Quantum information geometry of driven CFTs. *J. High Energy Phys.* **2023**, 087 (2023).

[34] K. Gawędzki and K. K. Kozlowski. Full counting statistics of energy transfers in inhomogeneous nonequilibrium states of (1+1)D CFT. *Commun. Math. Phys.* **377**, 1227 (2020).

[35] X. Liu, A. McDonald, T. Numasawa, B. Lian, and S. Ryu. Inhomogeneous quantum quenches of conformal field theory with boundaries. *Phys. Rev. Lett.* **134**, 220404 (2025).

[36] P. Moosavi, M. Christandl, G. M. Graf, and S. Sotiriadis. Perfect wave transfer in continuous quantum systems. arXiv:2408.00723 [quant-ph] (2024).

[37] K. Goto, M. Nozaki, S. Ryu, K. Tamaoka, and M. T. Tan. Non-equilibrating a black hole with inhomogeneous quantum quench. *J. High Energy Phys.* **2025**, 186 (2025).

[38] S. Das, B. Ezhuthachan, A. Kundu, S. Porey, B. Roy, and K. Sengupta. Brane detectors of a dynamical phase transition in a driven CFT. *SciPost Phys.* **15**, 202 (2023).

[39] P. Caputa and D. Ge. Entanglement and geometry from subalgebras of the Virasoro algebra. *J. High Energy Phys.* **2023**, 159 (2023).

[40] C. Bai, A. Miyata, and M. Nozaki. Entanglement dynamics in 2d HCFTs on the curved background: the case of q-Möbius Hamiltonian. *J. High Energy Phys.* **2024**, 208 (2024).

[41] H. Jiang and M. Mezei. New horizons for inhomogeneous quenches and Floquet CFT. *J. High Energy Phys.* **2025**, 025 (2025).

[42] G. D. Giulio and E. Tonni. Complexity of mixed Gaussian states from Fisher information geometry. *J. High Energy Phys.* **2020**, 101 (2020).

[43] P. Caputa and J. M. Magan. Quantum computation as gravity. *Phys. Rev. Lett.* **122**, 231302 (2019).

[44] J. Erdmenger, J. Kastikainen, and T. Schuhmann. Towards complexity of primary-deformed Virasoro circuits. *J. High Energy Phys.* **2025**, 127 (2025).

[45] M. V. Berry. Quantal phase factors accompanying adiabatic changes. *Proc. Roy. Soc. Lond. A* **392**, 45 (1984).

[46] M. O. Scully and M. S. Zubairy. *Quantum Optics*. Cambridge University Press, Cambridge (1997).

[47] J. E. Avron, R. Seiler, and P. G. Zograf. Viscosity of quantum Hall fluids. *Phys. Rev. Lett.* **75**, 697 (1995).

[48] P. Lévay. Berry phases for Landau Hamiltonians on deformed tori. *J. Math. Phys.* **36**, 2792 (1995).

[49] B. Oblak, B. Lapierre, P. Moosavi, J.-M. Stéphan, and B. Estienne. Anisotropic quantum Hall droplets. *Phys. Rev. X* **14**, 011030 (2024).

[50] P. Moosavi, B. Oblak, B. Lapierre, B. Estienne, and J.-M. Stéphan. Quantum Hall edges beyond the plasma analogy. *Phys. Rev. Res.* **7**, 023134 (2025).

[51] B. Oblak and B. Estienne. Adiabatic deformations of quantum Hall droplets. *SciPost Phys.* **15**, 159 (2023).

[52] T. Ozawa and N. Goldman. Extracting the quantum metric tensor through periodic driving. *Phys. Rev. B* **97**, 201117 (2018).

[53] B. Oblak. Berry phases on Virasoro orbits. *J. High Energy Phys.* **2017**, 114 (2017).

[54] R. Goodman and N. R. Wallach. Structure and unitary cocycle representations of loop groups and the group of diffeomorphisms of the circle. *J. R. Angew. Math.* **347**, 69 (1984).

[55] R. Goodman and N. R. Wallach. Projective unitary positive-energy representations of $\text{Diff}(S^1)$. *J. Func. Anal.* **63**, 299 (1985).

[56] M. Schottenloher. *A Mathematical Introduction to Conformal Field Theory*. Springer, Berlin, Heidelberg (2008).

[57] E. Witten. Coadjoint orbits of the Virasoro group. *Commun. Math. Phys.* **114**, 1 (1988).

[58] P. Di Francesco, P. Mathieu, and D. Sénéchal. *Conformal Field Theory*. Springer, New York (1997).

[59] L. J. Boya, A. M. Perelomov, and M. Santander. Berry phase in homogeneous Kähler manifolds with linear Hamiltonians. *J. Math. Phys.* **42**, 5130 (2001).

[60] R. Kubo. Statistical mechanical theory of irreversible processes. 1. General theory and simple applications in magnetic and conduction problems. *J. Phys. Soc. Jap.* **12**, 570 (1957).

[61] G. Bräunlich, G. M. Graf, and G. Ortelli. Equivalence of topological and scattering approaches to quantum pumping. *Commun. Math. Phys.* **295**, 243 (2010).

[62] J. E. Avron, M. Fraas, G. M. Graf, and P. Grech. Adiabatic theorems for generators of contracting evolutions. *Commun. Math. Phys.* **314**, 163 (2012).

[63] C. C. Gerry. Dynamics of $SU(1, 1)$ coherent states. *Phys. Rev. A* **31**, 2721 (1985).

[64] J. Zalesny. Time evolution of $SU(1, 1)$ coherent states. *Acta Phys. Polon. A* **98**, 11 (2000).

[65] M. Born and V. Fock. Beweis des Adiabatensatzes. *Z. Phys.* **51**, 165 (1928).

[66] B. Oblak and G. Kozyreff. Berry phases in the reconstructed KdV equation. *Chaos* **30**, 113114 (2020).

[67] B. Oblak. Topological bifurcations and reconstruction of travelling waves. *Phys. Fluids* **33**, 027107 (2021).

[68] B. Lapierre, K. Choo, A. Tiwari, C. Tauber, T. Neupert, and R. Chitra. Fine structure of heating in a quasiperiodically driven critical quantum system. *Phys. Rev. Res.* **2**, 033461 (2020).

[69] D. Das, R. Ghosh, and K. Sengupta. Conformal Floquet dynamics with a continuous drive protocol. *J. High Energy Phys.* **2021**, 172 (2021).

[70] P. M. Schindler and M. Bukov. Geometric Floquet theory. *Phys. Rev. X* **15**, 031037 (2025).

[71] A. Uhlmann. Parallel transport and “quantum holonomy” along density operators. *Rep. Math. Phys.* **24**, 229 (1986).

[72] A. Uhlmann. Gauge field governing parallel transport along mixed states. *Lett. Math. Phys.* **21**, 229 (1991).

[73] A. M. Perelomov. Generalized coherent states and some of their applications. *Sov. Phys. Usp.* **20**, 703 (1977).

[74] A. Perelomov. *Generalized Coherent States and Their Applications*. Theoretical and Mathematical Physics. Springer, Berlin, Heidelberg (1986).

[75] P. van Moerbeke. The spectrum of Jacobi matrices. *Invent. Math.* **37**, 45 (1976).